TOPICAL REVIEW

Neutral gas depletion in low temperature plasma

IOP Publishing Journal of Physics D: Applied Physics

J. Phys. D: Appl. Phys. **50** (2017) 473002 (31pp) https://doi.org/10.1088/1361-6463/aa87a9

Topical Review

Neutral gas depletion in low temperature plasma

A Fruchtman

H.I.T.—Holon Institute of Technology, 52 Golomb St., Holon 58102, Israel

E-mail: fnfrucht@hit.ac.il

Received 5 November 2014, revised 17 July 2017
Accepted for publication 22 August 2017
Published 26 October 2017

Abstract

Neutral depletion can significantly affect the steady state of low temperature plasmas. Processes that lead to neutral depletion and the resulting plasma–neutrals steady state are reviewed. Two such processes are due to collisions of neutrals with plasma. One process is the drag by ions that collide with neutrals and push them towards the wall. Another process is neutral-gas heating by collisions with plasma that makes the gas hotter at the discharge center. These processes, which usually occur under (static) pressure balance between plasma and neutrals, are called here 'neutral pumping'. When collisions are negligible, neutrals that move ballistically between the chamber walls are depleted through ionization, a process called here 'ion pumping'. The effect of the magnetic field on neutral depletion is explored in plasma in which the dynamics is governed by cross-field diffusion. Finally, neutral depletion in a flowing plasma is analyzed.

Keywords: gas heating, cross-field transport, helicon plasma thruster, particle balance, neutral depletion

(Some figures may appear in colour only in the online journal)

1. Introduction

Low temperature plasmas, such as those in gas discharges and in industrial plasmas, are usually weakly ionized, so that the neutral-gas density and temperature are not significantly affected by the plasmas [1–12]. When the power deposited in the plasma is increased, or when the neutral pressure is low, the plasma modifies the neutral density and temperature. Since the plasma dynamics depends on the neutral dynamics, the problem of solving for the plasma steady-state becomes inherently nonlinear. One result of the nonlinear dynamics is that particle balance and power balance become coupled. In the linear case, when the neutral density is not modified, particle balance is usually sufficient to determine the electron temperature, and power balance is employed to determine the plasma density. When the nonlinear coupled plasma–neutrals dynamics is modeled, particle balance and power balance have both to be taken into account in order to solve for the electron temperature and for the plasma density.

The main process that follows the coupling of plasma and neutral dynamics is neutral gas depletion [13–111], the decrease of neutral gas density where the plasma density is high, at the discharge center. As is common in the literature, neutral gas depletion is termed neutral depletion in this paper. Neutral depletion in gas discharges has already been addressed theoretically and many features were unfolded in early studies [13–26]. Allen and Tonemann related in 1954 the phenomenon of current limitation in a low pressure arc to neutral depletion [14]. In various models, collisionless neutrals were assumed to be ionized while moving ballistically, and the neutrals flow was described by moments of the distribution function. The first such model for neutral depletion in collisionless plasma was derived by Caruso and Cavaliere in 1964 for two counter-streaming monoenergetic neutral beams in a planar geometry [15]. The trajectories of neutral atoms in both planar and cylindrical geometries have been examined by Valentini [16] and by Torven [17] in 1971. Stangeby and Allen calculated, also in 1971, the neutral depletion in a cylindrical geometry

considering ionization of neutrals during their ballistic motion [18]. The plasma, though, was assumed of a uniform density in [18]. In research in the following years, Valentini used the Boltzmann equation to derive equations for the moments of the velocity distributions of both neutrals and ions with anisotropic pressures in planar and cylindrical geometries [22]. He then closed the hierarchy of fluid equations, by relating the heat flux tensor to the pressure tensor [25, 26]. Valentini took into consideration that an ion born through ionization had initially the velocity of the ionized neutral atom. Some ions were therefore shown to move initially toward the center of the discharge, against the electric force [23, 24]. The calculated neutral velocity in cylindrical geometry when plasma was assumed collisional was found sometimes to be radially nonmonotonic [25]. Early measurements of neutral depletion are summarized in chapter 5.1 of [8].

In recent years, with the growing use of lower pressure and higher power radio-frequency (rf) discharges, the importance of neutral depletion is becoming fully recognized [27–111]. A variety of aspects of neutral depletion have been explored experimentally. Boswell *et al* [27, 28] and Gilland *et al* [40] suggested the possibility of neutral depletion in helicon sources. Degeling *et al* [42] found breathing oscillations that were associated with oscillating neutral depletion. Decrease of the neutral density [27–40, 48, 68–71, 81, 82], relaxation oscillations [42], and neutral-gas heating [54–61, 64, 67, 75, 81, 82, 87] have been measured. The experiments were often accompanied by detailed numerical modeling.

The experimental findings have stimulated renewed theoretical research [33, 34, 42, 46, 62, 72, 74, 77, 79, 80, 85, 86, 88–90, 94]. Modeling the full range of processes in such experiments is a difficult task. Often in partially ionized plasmas there are several atomic and molecular species. The description of the populations of the many excited states can be complex, even in a global model [108]. When the spatial dependence is taken into account, the analysis is even more complex. When the pressure is low, so that neutral collisions are rare, kinetic modeling is more accurate than hydrodynamic modeling. Combinations of hydrodynamic and Monte Carlo techniques are often used [33, 34]. For example, in a simulation of an electron cyclotron resonance (ECR) plasma reactor, a direct simulation Monte Carlo (DSMC) was employed. The neutral density was indeed found to be depleted in the volume of the chamber due to ionization and the depletion was enhanced by neutral heating by electron–neutral and ion–neutral collisions [34].

In this review paper, we examine neutral depletion in low temperature plasmas theoretically, under simplifying assumptions. The theory used here cannot simulate experiments with accuracy, as the abovementioned detailed computational models can sometimes do. Our theoretical study with the simplifying assumptions, somewhat in the spirit of the early theoretical studies, but often with simpler analysis and with less detail, enables us to demonstrate characteristic phenomena and (sometimes unexpected) behavior of the plasma under neutral depletion. Most of the results described here have been published in the last two decades, while some results are new.

We focus on the theoretical analysis of neutral-depleted steady-states of low temperature plasmas. We address discharges with one species only, in which the plasma is composed of one type of neutrals, (positive) ions all of the same degree of ionization, and electrons. Moreover, in order to exhibit the various different behaviors of neutral-depleted plasma, we treat discharge configurations under idealized assumptions about ion and neutral collisionality, and about plasma and neutral equations of state. Most of the discussion is of neutral depletion in non-flowing plasmas, with a brief discussion of neutral-depleted flowing plasma. Different processes that lead to neutral depletion are distinguished. Neutrals are depleted either due to the pushing of neutrals by ions that move from the center of the discharge towards the walls under electron pressure, due to ionization, or due to gas heating by the plasma. These processes occur in unmagnetized and in magnetized plasmas. The relation between processes that lead to neutral depletion and pressure balance is pointed out.

In section 2 measurements in low temperature plasmas that indicate neutral depletion are briefly described. The measurements described were taken in rf discharges over the last several decades.

In section 3, the general governing equations are presented. For simplicity, we restrict ourselves mostly to a steady state one-dimensional (1D) slab-geometry plasma bounded by walls. Discharges of cylindrical geometry and flowing plasmas are also treated in some cases.

Unmagnetized plasma is addressed first. In section 4, a relation between the electron temperature and the total number of neutrals per unit area is derived, a generalization of the known relation for uniform-density neutrals. In section 5, plasma and neutrals that are collisional and in (static) pressure balance are discussed. In such collisional plasma, neutral depletion results from both plasma (usually electron) pressure and neutral-gas heating by the plasma [24, 26, 62, 72, 74, 77, 78]. Neutral depletion in a collisional plasma due to electron pressure follows the drag force that plasma and neutrals exert on each other due to mutual ion–neutral collisions. We call the depletion of neutrals due to such collisions neutral pumping [62, 77, 78]. Analytical relations are derived, and a nonmonotonic dependence of the plasma density on the plasma particle flux is shown. Such a nonmonotonic dependence is demonstrated numerically in cylindrical geometry as well.

In addition to plasma (electron) pressure, neutral-gas heating also leads to neutral depletion [24, 26, 74, 78]. Neutral heating by the plasma results in a non-uniform gas temperature. Even if plasma pressure is negligible so that neutral pressure is uniform, the higher gas temperature at the discharge center should cause neutral depletion there, a reduced neutral density. Neutral depletion due to neutral-gas heating is discussed in section 6. In this paper, neutral heating by collisions is balanced by neutral heat conduction, while the heat flux is proportional to the neutral temperature gradient [74, 78]. The relations between the neutral depletion and the neutral temperature is explored for planar and cylindrical geometry. Nonmonotic dependencies of the plasma density and of the neutral temperature on the plasma flux density (and deposited wave power) are shown.

The process which we coin ion pumping [77] is the removal of neutrals by ionization instead of by collisions with ions (as in neutral pumping). Ion pumping is dominant when ions and neutrals do not collide, so that plasma and neutrals are coupled through ionization only. Ion pumping, described in

section 7, is the mechanism for neutral depletion when ions and neutrals are collisionless [15, 16, 24, 77, 78, 90].

Neutrals of low density that do not collide between themselves so that they are not thermalized, but rather move ballistically between the chamber walls, can still be depleted when ions collide with them, pushing them towards the wall [78]. This happens if the mean free path of an ion between its collisions with neutrals is smaller than the mean free path for a neutral between its collisions with other neutrals. This different type of neutral pumping is described in section 8.

The possibility that, due to ionization, neutral density becomes larger at the discharge center than near the wall—termed 'repletion'—that has been suggested in [72, 79, 89], is examined in section 9. We conclude that it is not likely that repletion can occur.

In section 10, we turn to magnetized plasma. The effect of the magnetic field on neutral depletion is explored in plasma in which the flow is ambipolar and the dynamics is governed by cross-field diffusion. The question of ambipolarity in magnetized discharge is controversial, as the short-circuit effect is often claimed to allow nonambipolar flow across magnetic field lines [85, 94, 107, 112, 113]. Indeed, in [85], plasma and neutral steady-state with depleted neutrals was analyzed for both ambipolar and nonambipolar cross-field diffusions. Here, we study the case of ambipolar cross-field diffusion only. Electrons cross magnetic field lines due to collisions either with neutrals or with ions. We examine separately how these two types of collision affect neutral depletion and the magnetized plasma. The question that is addressed here is how neutral depletion varies when the intensity of the magnetic field varies. We discover that neutral depletion varies differently when either plasma density or plasma particle flux density is kept constant when the magnetic field varies. We also present the result of a recent study that has found that neutral depletion suppresses diamagnetism [114].

Flowing plasmas are also affected by neutral depletion. Neutral depletion is important in plasma thrusters [77, 115–133] in which both plasma and neutrals are flowing. Neutral depletion in a flowing plasma is described briefly in section 11.

Research has revealed how neutral depletion plays a role in configurations not analyzed in this paper. Neutral depletion may lead to time-dependent phenomena, such as breathing oscillations [42, 43]. Sometimes neutral depletion is an inherently two-dimensional (2D) phenomenon, especially in magnetized plasma [40, 88]. Neutral dynamics and neutral depletion are also important in the divertor of the Tokamak [84] and in negative-ion sources [91–93, 103–105]. Finally, unbounded plasma that is terminated at neutral gas often occurs in nature [99]. These more complex phenomena require more detailed, and often numerical, analysis for modeling, but the analysis presented here could be a useful guide.

2. Measurement of neutral depletion

Early measurements of neutral depletion in DC discharges are described in [8]. Here, we describe the later measurements of neutral depletion, mostly in rf discharges.

The first experiments with rf discharge that showed neutral depletion were probably those by Boswell *et al* [27, 28], who used measured Doppler broadening of lines in an argon helicon plasma source to deduce ion and neutral temperatures. They found that the Ar atoms temperature was about 3000 K at the center of the discharge, while near the discharge edges it was 300 K. Assuming that the gas was in pressure balance (not necessarily coupled to the plasma pressure), they concluded that the gas density at the discharge center was ten times lower than near the edge. Boswell mentioned that this large decrease of gas density at the center, when occurring in pulsed gas lasers, was called gas pumping [28]. Later, Porteous and Boswell have simulated an ECR source including neutral transport and identified neutral depletion due to both ionization and gas heating [29].

In the following studies, various methods were used to measure gas temperature in discharges, because of the significant effect of gas temperature gradients on density distribution and transport of reactive free radicals. In certain studies, neutral density was measured as well. Here, we mention some of these studies.

Gorbatkin *et al* measured the pressure in the ECR source and downstream using magnetically shielded capacitance manometers, and found about threefold pressure difference [30]. Rossnagel *et al* measured the electron density in an argon ECR source with a microwave interferometer device [31]. They found that when rf power of 1250 W was applied to the gas—which was initially at 0.7 mTorr—the gas density was reduced to 14% of its value without the discharge. They related the neutral depletion to gas heating to 2500 K temperature, which they found consistent with temperature measurements based on Doppler broadening. Nakano *et al* used high-resolution laser-induced fluorescence (LIF) to determine the temperature of neutrals in an ECR source [32]. They found that the neutral temperature was 800 K in the source and only 350 K downstream. Hebner [35] measured neutral heating in an argon inductively coupled plasma (ICP). Even at moderate power of 200W, the temperature reached 900 K. Hori *et al* [36] measured the radial neutral density profile in argon ICP, by Thomson and Rayleigh scattering of laser light. They found neutral depletion up to 40%, which was explained by gas heating due to collisions of neutrals with charged particles. Lee and Chang [37] used an optical probe technique in an argon ECR to identify neutral depletion. The neutral depletion was also explained by gas heating due to ion-neutral collisions. Clarenbach *et al* [59] employed time-resolved laser absorption spectroscopy, and later also a collisional-radiative (CR) code [71] (based on [134, 135]). Assuming a strong coupling, such that the temperature of the metastable atoms reflects the gas temperature, they deduced the density of the ground-state argon atoms, and found that in high density argon helicon sources the gas temperature can reach 1000 K, and neutral atoms can be depleted by more than a factor of ten. Sudit *et al* [38, 39] estimated the neutral depletion by the difference between the plasma-off and the plasma-on pressures. Gilland *et al* [40] measured the neutral pressure in the bulk of a helicon discharge using temperature-controlled capacitive manometer gauge, and showed the dependence on wave power and on the initial fill pressure. They found that the neutral pressure decreased by a factor up to ten compared to the pressure before the discharge. Neutral depletion was assumed

to be caused by ionization, called neutral pumping in [40] (here named ion pumping). Miljak and Chen [41] attributed an observed plasma density limit in a high-power helicon discharge to gas depletion.

Neutral-gas heating often occurs in discharges with molecular gases. Booth *et al*, while using LIF in capacitive coupled CF_4 plasma, did not find elevated gas temperature, probably because the plasma density was not high enough [44]. Abada *et al* [55] measured the gas temperature in a CF_4 inductive discharge of a higher plasma density. They did find higher gas temperatures at the discharge center (up to 800 K). They have shown, both by a global thermal model and by a two dimensional model, that heating by electrons (rather than by ions) explains the measured gas heating. Heat conduction by the neutrals towards the wall was assumed to balance the gas heating. The plasma electrons were found to excite a certain vibrational mode of CF_4. Assuming that there was a sufficiently fast relaxation of this energy into other modes, they concluded that this excitation was the dominant electron–neutral collision process [55].

Tynan [46] measured a reduction of neutral pressure at the center of ICP and helicon discharges. Tynan and his colleagues [46, 48] explained the reduction as neutral depletion that is caused by plasma (ion) pumping, neutral evacuation through ionization. In later research by the same group, Shimada *et al* [76] used an improved technique of measuring pressure that was suitable for rarefied gases too, and measured neutral temperature and pressure in Ar/5% N_2 ICP. They found that the total pressure was uniform, while neutral pressure was lower at the discharge center. They were thus able to show that neutral depletion resulted from both gas heating and electron pressure. Shimada *et al* [80] then used a hybrid-type DSMC method for a 1D cylindrical electrostatic plasma in Ar/N_2 mixtures to simulate the experiment. In the simulated plasma, the pressure was too high for plasma (ion) pumping to be dominant. Plasma pressure and gas heating were identified as the major sources for neutral depletion. In the simulated gas mixture, a major source for argon gas heating was collisions with Franck–Condon dissociated nitrogen atoms [80]. The relative dominance of each type of collision, argon ion and neutral atom versus hot (due to dissociation) nitrogen atom and argon atom, was determined in the simulations. As expected, when the nitrogen partial pressure was larger, the heating due to Franck–Condon dissociated atoms was also larger. Near the wall, heating by ion collisions was larger.

At the University of Bochum, O'Connell *et al* [81, 82] were conducting experiments on an ICP source that could operate at lower pressure than other ICP sources. Gas temperature was determined from Doppler profiles of diode laser absorption measurements on metastable argon. Gas temperature was shown to increase significantly with both power and pressure; it reached up to 1500 K at 5 Pa and 2000 W. O'Connell *et al* were able to distinguish in their measurements between depletion due to electron pressure and depletion due gas heating. Their conclusions were supported by Crintea *et al* [87], who used an optical emission spectroscopy (OES) technique together with Thomson scattering for the determination of electron temperatures and densities in those low-pressure argon discharges. The dominance of each of the two depletion mechanisms was associated with the fill pressure. At a lower pressure (lower than 0.1 Pa in their experiment), intense ionization resulted in electron pressure comparable to the gas pressure, which led to a significant neutral depletion. At a higher pressure, gas heating was the dominant depletion mechanism. It was demonstrated that because depletion due to electron pressure decreases while depletion due to gas heating increases when gas pressure is increased, the dependence of the depletion on the gas pressure is not monotonic. In their measurements, depletion first decreased and later increased when gas pressure was increased [81, 82, 87].

Scime's group has explored various aspects of neutral depletion [68, 70, 95, 96, 98, 106]. Keesee *et al* [68, 70] combined LIF measurements of excited neutral atom states with a CR model (based on [134, 135]) to extract the density profile of the ground state depleted (up to 60%) neutral atoms. The technique was employed further to demonstrate how the ionization fraction and neutral depletion significantly depend on the gas pumping [95]. Magee *et al* [96] developed a two photon absorption laser induced fluorescence (TALIF) diagnostic for measuring neutral density. They showed in a krypton helicon source that neutral depletion increased while neutral temperature decreased when the magnetic field was increased. They concluded that neutral depletion in this case does not follow gas heating but is, rather, a result of ion pumping. Dominant plasma motion was assumed along, and not across, magnetic field lines in this study. Magee *et al* [98] then performed fast time-resolved measurements of the neutral density in the helicon source. They found a fast decrease of the neutral density in the high electron temperature plasma near the antenna and about a thousand times slower neutral depletion in the lower temperature plasma downstream. They conjectured that the neutral depletion near the antenna was due to high ionization (ion pumping), while downstream it was due to pushing by energetic ions (neutral pumping). Galante *et al* [106] found with the TALIF diagnostic method that, contrary to the large neutral depletion in krypton, neutral depletion in hydrogen and deuterium was negligible.

Aanesland *et al* [75] were probably the first to measure neutral depletion using TALIF, following a proposal to use the technique by O'Connell *et al* [69]. With TALIF, Aanesland *et al* [75] measured directly the ground state neutral density in a xenon helicon source. Neutral depletion was found to increase with magnetic field intensity (as was also found in [96]). The sum of plasma pressure and gas pressure (assuming no gas heating) was lower on axis than near the wall. It was suggested that elevated gas temperature or the inclusion of magnetic pressure could recover pressure balance. They also found out that the total number of neutrals was lower during the discharge. That last finding was explained by Liard *et al* [97] who used time-resolved TALIF to show that the pumping efficiency was higher when the magnetized plasma column was ignited.

Denning *et al* [83] observed neutral depletion in a flowing high-power (up to 3 kW) argon helicon plasma. For plasma diagnostics they used microwave interferometry, a double Langmuir probe and optical spectroscopy, together with a CR code. The measured plasma parameters, spectroscopic measurements, and a CR code (as in [68]) were used to determine the neutral density. A decrease of neutral density along the flow was found, a decrease that was more dramatic for a higher wave power. The upstream plasma density increased with power until saturation,

but the downstream plasma density did not increase much with power. The asymmetry of the plasma density profile along the flow in a helicon plasma source was measured further with a Langmuir probe by Takahashi *et al* [109] for argon, krypton and xenon discharges. They suggested that this asymmetry in plasma density was related to neutral depletion, as was predicted theoretically [77], and that the asymmetry affected the axial momentum loss at lateral walls. In a following study, Takahashi *et al* [111] indeed measured the neutral density in an argon helicon source. They used a Langmuir probe for the plasma density, together with measurement of optical emission—that is proportional to the product of neutrals and plasma densities. Their measurements in a 2.5 ms pulsed discharge indicated that the neutral density first decreased due to fast ionization in less than 100 μs, and then the maximum of the plasma density moved backwards towards the gas inlet over about 250 μs, establishing the axially asymmetric plasma density profile.

Plasma relaxation oscillations have been measured in a large volume helicon source, and were associated with neutral depletion [42, 43]. Degeling *et al* [43] found that the plasma density oscillates between high and low-density modes. The oscillations had a period of several milliseconds, and have been identified as transitions between a low-density, inductive discharge and a high-density, helicon-wave discharge. Degeling *et al* [42] showed by a theoretical model that the mode transitions could be triggered by variations in the neutral density in the source region. The neutral density decreased due to ionization augmented by ion pumping, and increased due to refilling of the source chamber from the much larger diffusion chamber.

Delivering energy and momentum to neutral gas for space propulsion is often considered (usually, without examining the effect on the neutral density). At the Australian National university, a rf electrothermal microthruster has been developed [119, 130], named the mini pocket rocket, in which gas pressure was increased through neutral heating by the plasma. The gas temperature was measured by OES [119]. Makrinich and Fruchtman used a balance-force-meter to measure the momentum delivered to neutrals by accelerated ions [116, 120].

Cooper and Gekelman [99] studied a neutral boundary layer in which a magnetized plasma terminates on a neutral gas in the direction of the magnetic field without touching a solid surface. The experiments were performed at the Enormous Toroidal Plasma Device at UCLA. The plasma parameters and the potential were measured by various probes. The presence of an ambipolar electric field and pressure equilibration were reported [99].

3. The governing equations

We assume a steady-state quasi-neutral plasma in which volume ionization is balanced by recombination at the walls. For simplicity and in order to derive analytical results, we consider in a large part of the paper a 1D slab geometry in which all variables depend on x only. The plasma is assumed to be bounded by walls at $x = \pm a$ and that there is symmetry with respect to the plane $x = 0$. There might be a uniform magnetic field in the z direction of intensity B. When a slab geometry is assumed it replaces, in our model, the more realistic cylindrical geometry of a magnetized plasma discharge. In several cases, cylindrical geometry is addressed, where variables depend on the distance r from the axis of symmetry, and the wall is at $r = a$. The plasma flow in the x (or r) direction is assumed ambipolar, even when the flow is across a magnetic field. In section 11, an analysis of a flowing plasma with an open end is presented.

We describe the plasma and the neutral dynamics by fluid equations that allow us a unified simplified description of both collisional and collisionless cases. The one-fluid governing equations for the plasma in a planar geometry are the continuity equation

$$\frac{\mathrm{d}\Gamma}{\mathrm{d}x} = S, \tag{1}$$

and the momentum equation,

$$\frac{\mathrm{d}\left(mnv^2 + nT\right)}{\mathrm{d}x} = mSV - m\beta_c Nnv - \frac{m_e\omega_c^2}{\nu_e}\Gamma, \tag{2}$$

in which the inertia terms are retained. The source term S will usually be assumed to be of the form

$$S = \beta Nn. \tag{3}$$

Here, n and N are the density of the quasi-neutral plasma and the density of the neutral gas, v and V are the velocities of the plasma and neutral fluids, T is the (assumed uniform) electron temperature, m and m_e are the ion and electron masses, and

$$\Gamma \equiv nv \tag{4}$$

is the plasma particle flux density in the x direction. The ion temperature is assumed to be much smaller than the electron temperature, so that the plasma pressure is approximately the electron pressure. Otherwise, T should have been the sum of the electron temperature and the ion temperature. Also, β and β_c are the ionization and ion–neutral collision rate coefficients, ν_e is the electron collision frequency, and $\omega_c \equiv eB/m_e$ is the electron cyclotron frequency (e is the elementary charge). The contribution of the magnetic field is expressed by the last term on the right-hand side (RHS) of equation (2) when $\omega_c \gg \nu_e$. We consider the magnetic field only at this limit.

The momentum equation for the plasma, equation (2), is the sum of the separate equations of motion for ions and for electrons. An ambipolar electric field arises in the plasma that exerts equal and opposite forces on the (positive) ions and on the electrons in the quasi-neutral plasma. The net electric force on the plasma is zero, and therefore the electric force does not appear in equation (2).

The governing equations for the neutral gas are the continuity equation

$$\frac{\mathrm{d}\Gamma_N}{\mathrm{d}x} = -S, \tag{5}$$

and the momentum equation

$$\frac{\mathrm{d}\left(mNV^2 + p_N\right)}{\mathrm{d}x} = -mSV + m\beta_c Nnv. \tag{6}$$

Here, $\Gamma_N \equiv NV$ is the neutral particle flux density in the x direction, and p_N is the neutral-gas pressure, for which we specify forms later.

The first term on the RHS of equation (2) is the momentum of neutrals being ionized—that is added to the momentum of

the ion fluid—while the first term on the RHS of equation (6) is the same momentum that is subtracted from momentum of the neutral fluid (see the derivation using Boltzmann equation in appendix A of [72]). The second term on the RHS of equations (2) and (6) is the drag on ions and neutrals due to their mutual collisions. In writing the drag due to ion–neutral collisions, we assume that the plasma density is considerably smaller than the neutral density (although their pressures might be comparable), so that the plasma velocity is much larger than the neutral velocity,

$$n \ll N, \quad |v| \gg |V|. \tag{7}$$

Therefore, the drag—the ion–neutral friction force—that should be proportional to the relative velocity between ions and neutrals, is taken as proportional to the ion (plasma) velocity. Because $|v| \gg |V|$, we neglect in all the cases treated here the first term on the RHS of equation (2). When the net mass flow is zero, $\Gamma + \Gamma_N = 0$, the following relation

$$\Gamma_N = -\Gamma, \tag{8}$$

holds. The plasma flows towards the wall, while neutrals flow from the wall towards the discharge center. Correspondingly, for $0 \leqslant x \leqslant a$, v is positive while V is negative. In section 11, we discuss the case of a flowing plasma, in which the net mass flow is not zero, so that equation (8) does not hold.

The contributions of ionization and collisions to the total momentum of the neutrals, expressed by the two terms on the RHS of equation (6), are positive (for $0 \leqslant x \leqslant a$) and, as a result, the total momentum of the neutrals increases monotonically from the symmetry plane at $x = 0$ towards the walls at $x = \pm a$. This larger total momentum at the wall holds for both collisional and collisionless neutrals, and for every form of p_N.

Ampere's law is written as

$$\frac{\partial B}{\partial x} = \mu_0 e \frac{\omega_c}{\nu_e}\Gamma, \tag{9}$$

where μ_0 is the vacuum permeability. Summing equations (2) and (6) with the use of equation (9), we obtain pressure balance between plasma pressure, neutrals pressure and magnetic pressure,

$$mnv^2 + nT + mNV^2 + p_N + \frac{B^2}{2\mu_0} = p_r. \tag{10}$$

Here, p_r is the uniform total pressure. With the use of equation (8) and the assumption that ions reach the ion acoustic velocity (or the Bohm velocity [3]),

$$c \equiv \left(\frac{T}{m}\right)^{1/2}, \tag{11}$$

at the wall vicinity (at the plasma-sheath boundary), the total pressure p_r is written as

$$p_r = \left(2 + \frac{n_W}{N_W}\right) n_W T + p_{N,W} + \frac{B_W^2}{2\mu_0}. \tag{12}$$

Here, n_W, N_W, and $p_{N,W}$ are the plasma density, the neutral density, and the neutral pressure near the wall, at the plasma-sheath boundary (see, for example, [22, 110]).

The equations can be written in an equivalent useful form. Combining the continuity and momentum equations above, we write the momentum equation as

$$mnv\frac{\mathrm{d}v}{\mathrm{d}x} + \frac{\mathrm{d}\left(nT\right)}{\mathrm{d}x} = mS(V - v) - m\beta_c Nnv - \frac{m_e\omega_c^2}{\nu_e}\Gamma, \tag{13}$$

for the plasma, and as

$$mNV\frac{\mathrm{d}V}{\mathrm{d}x} + \frac{\mathrm{d}p_N}{\mathrm{d}x} = m\beta_c Nnv, \tag{14}$$

for the neutrals. In the case that

$$p_N = p_N(N), \tag{15}$$

equation (14) is written as

$$mNV\frac{\mathrm{d}V}{\mathrm{d}x} + \frac{\mathrm{d}p_N}{\mathrm{d}N}\frac{\mathrm{d}N}{\mathrm{d}x} = m\beta_c Nnv. \tag{16}$$

Using equations (5) and (16), we express the spatial derivative of the neutral density as

$$\left(\frac{1}{m}\frac{\mathrm{d}p_N}{\mathrm{d}N} - V^2\right)\frac{\mathrm{d}N}{\mathrm{d}x} = \left(\frac{S}{N} - \beta_c N\right)\Gamma_N. \tag{17}$$

In addition to the assumptions in equation (7), we assume that v is smaller than the neutral thermal velocity, so that the friction force is linear in v. Otherwise, the case discussed by Godyak of a friction proportional to v^2 should be considered [9]. Therefore, here, β_c, the ion–neutral collision rate constant, is taken as constant. For argon, it is about $\beta_c = 6.3 \times 10^{-16}$ m^3 s^{-1} (chapter 3 in [10]).

We note that in equation (17) there are four terms, two terms on the left-hand side (LHS) and two terms on the RHS. When different terms are dominant, the behavior of the neutrals is different. While equation (6) showed that the total neutral pressure increases towards the wall, the terms in brackets in equation (17) can be either positive or negative, and it is not clear *a priori* whether the neutral density increases or decreases towards the wall.

The ionization rate coefficient, β, is approximated as (p 79 in [10])

$$\beta = \sigma_0 v_{te}\left(1 + \frac{2T}{\epsilon_i}\right)\exp\left(-\frac{\epsilon_i}{T}\right), \tag{18}$$

where $v_{te} \equiv \left(8T/\pi m_e\right)^{1/2}$ is the electron thermal velocity and $\sigma_0 \equiv \pi\left(e^2/4\pi\epsilon_0\epsilon_i\right)^2$, ϵ_0 being the vacuum permittivity and ϵ_i the ionization energy. For example, for argon, $\sigma_0 = 2.67 \times 10^{-20}$ m^2 and $\epsilon_i = 15.6$ eV. We note that β depends strongly on T, and often the electron temperature is determined once the value of β is specified.

Our interest in this paper is to calculate the rate of neutral-gas depletion in various cases. We define the neutral-gas depletion as

$$D \equiv 1 - \frac{N_0}{N_W}, \tag{19}$$

where N_W is the neutral density at the wall and $N_0 = N(x = 0)$ is the neutral density at the plane of symmetry at the center of the discharge. We note that this definition is different from the definition we used previously [77, 78]. The depletion varies between

$$0 \leqslant D \leqslant 1. \tag{20}$$

and its maximal value is unity.

4. Unmagnetized plasma—electron temperature and the number of neutrals

In this section, several general relations for unmagnetized plasma, $B = 0$, are presented. In weakly-ionized plasma, in which neutral-gas density is uniform, there is a well-known relation between the electron temperature T and the product of neutral density and the plasma spatial extent, Na [1–12]. Here, this relation is generalized to a discharge of nonuniform neutral density due to neutral depletion. The generalization is made, though, for an unmagnetized plasma in a planar geometry only. It is shown that in this more general case of nonuniform neutral density, T is related to the total number of neutrals (per unit area) in the discharge, $\int_{-a}^{a} N(x)\mathrm{d}x$ (which is reduced to $2Na$ for a uniform neutral density). In addition, we derive relations between the plasma particle flux density and the plasma density that in fact also hold when neutral density is not uniform. These relations for nonuniform neutral density are derived in more detail in [78].

The plasma governing equations for an unmagnetized plasma are the continuity equation, equation (1), and the momentum equation, equation (2), which becomes

$$\frac{\mathrm{d}\left(mnv^2 + nT\right)}{\mathrm{d}x} = -m\beta_c Nnv. \tag{21}$$

As explained above, the first term on the RHS of equation (2) has been neglected. Equations (1) and (21) are used to derive relations between the plasma particle flux density Γ and n, that are independent of N. For the derivation, we combine the two equations and obtain the relation

$$\frac{\mathrm{d}\ln\Gamma}{\mathrm{d}M^2} = \frac{\left(1 - M^2\right)}{2M^2\left[1 + M^2\left(1 + \beta_c/\beta\right)\right]}, \tag{22}$$

in which

$$M \equiv \frac{v}{c} \tag{23}$$

is the plasma Mach number. Note that the neutral density does not appear in Equation (22); therefore, the relations that are subsequently derived also hold for a discharge with nonuniform neutral density. Equation (22) shows that the plasma particle flux density does not grow with the velocity beyond $M = 1$. As mentioned above, we assume that the Mach number is unity at the plasma-sheath boundary near the wall. Equation (22) is integrated, and the plasma particle flux density, the plasma density, and the Mach number are related through

$$\Gamma = ncM, \qquad n = \frac{n_0}{\left[1 + M^2\left(1 + \beta_c/\beta\right)\right]^{\frac{1}{2}\left(1 + \frac{1}{1+\beta_c/\beta}\right)}}. \tag{24}$$

Here, n_0 is the maximal plasma density (where the plasma flow velocity is zero). The maximal plasma particle flux density and the minimal plasma density, both at the plasma boundary, are

$$\Gamma_{\max} = n_{\min}c, \quad n_{\min} = \frac{n_0}{\left(2 + \beta_c/\beta\right)^{\frac{1}{2}\left(1 + \frac{1}{1+\beta_c/\beta}\right)}}. \tag{25}$$

Eliminating M from the equations, we write the relation between Γ and n as

$$\Gamma_n^2 = \frac{\left(2 + \beta_c/\beta\right)^{(2+\beta_c/\beta)/(1+\beta_c/\beta)}}{\left(1 + \beta_c/\beta\right)}\left[n_n^{2/(2+\beta_c/\beta)} - n_n^2\right], \tag{26}$$

where

$$\Gamma_n \equiv \frac{\Gamma}{\Gamma_{\max}}, \quad n_n \equiv \frac{n}{n_0}. \tag{27}$$

We now use the relations between Γ and n, together with equations (1) and (3), to derive a relation between the electron temperature and the total number of neutrals (per unit area). From equation (1) we obtain

$$-\frac{M}{\left(1 + \beta_c/\beta\right)} + \frac{\left(2 + \beta_c/\beta\right)}{\left(1 + \beta_c/\beta\right)^{3/2}}\arctan\left[\left(1 + \frac{\beta_c}{\beta}\right)^{1/2} M\right] = \frac{\beta}{c}\int_0^x N\left(x'\right)\mathrm{d}x', \tag{28}$$

and, therefore,

$$-\frac{2}{\left(1 + \beta_c/\beta\right)} + 2\frac{\left(2 + \beta_c/\beta\right)}{\left(1 + \beta_c/\beta\right)^{3/2}}\arctan\left[\left(1 + \frac{\beta_c}{\beta}\right)^{1/2}\right] = \frac{\beta}{c}N_T, \tag{29}$$

where

$$N_T \equiv \int_{-a}^{a} N\left(x'\right)\mathrm{d}x'. \tag{30}$$

Relation (29) replaces the classical condition derived for the weakly-ionized case [1, 6]. Equation (29) relates the total number of neutrals per unit area N_T to the electron temperature T (through β and c). In the weakly-ionized case of uniform gas density N, the parameter N_T is reduced to the similarity variable $2Na$ [6], a similarity variable which is linearly related to the Paschen parameter, $p_N a$, in which p_N is the (assumed uniform) gas pressure. Thus the total number of particles N_T can be viewed as a generalized Paschen's parameter [62].

The bulky expression (29) is reduced to simpler expressions at the collisional and collisionless limits (the following equations (37) and (41)). These simpler expressions will be derived shortly.

We write the plasma momentum equation, equation (21), so as to exhibit the sonic singularity. Employing equations (1), (3) and (22), we write

$$\left(1 - M^2\right)\frac{\mathrm{d}M}{\mathrm{d}x} = \frac{\beta N}{c}\left[1 + M^2\left(1 + \frac{\beta_c}{\beta}\right)\right]. \tag{31}$$

We often relate the power deposited in the plasma to the rate of generation of electron–ion pairs through ionization. In a steady-state, this rate equals the outward plasma particle flux at the wall. In our 1D model, we write the relation [10, 11, 136],

$$P = \varepsilon_T(T)\Gamma_{\max}, \tag{32}$$

where P is the deposited power per unit area and $\varepsilon_T(T)$ is the energy necessary for generation of an electron–ion pair. This

energy includes the sum of the ionization energy, and other processes, and is a function of the electron temperature. The energy ε_T decreases with T for low T, and may increase with T for a higher T because of the energy deposited in ions in the sheath at the wall. Usually the power deposited in experimental system is known, but it is not clear whether P in equation (32) (multiplied by the area) is all that power, or only a part of the generator power. If P and T are known, we can use equation (32) to find $\Gamma_{\max}$, and from equation (25) we can find n_0.

The expressions above are bulky and we will derive simplified expressions for the special cases of collisional plasma and collisionless plasma. Note that the following relations in this section also hold for a discharge with a nonuniform neutral density.

4.1. Collisional plasma

For a collisional plasma,

$$\frac{\beta_c}{\beta} \gg 1, \tag{33}$$

we approximate

$$\Gamma_n^2 + n_n^2 = 1, \quad M = \left(\frac{\beta}{\beta_c}\right)^{1/2} \frac{\Gamma_n}{\sqrt{1-\Gamma_n^2}}, \quad \Gamma_{\max} = \Gamma_a \equiv n_0 c \left(\frac{\beta}{\beta_c}\right)^{1/2}, \tag{34}$$

so that when $\Gamma_n = 1$ at the wall, $n_{\min} = 0$ and the plasma velocity and M are infinite. As is shown below, within this diffusion approximation, additional physical quantities, such as the neutral heating rate, may become infinite at the wall. Whenever finite values for the ion velocity and for the heating rate are needed, we may take the values at the wall as the values that correspond to $M = 1$, which are

$$\Gamma_n(x=a) = \frac{1}{(1+\beta/\beta_c)^{1/2}} \cong 1 - \frac{\beta}{2\beta_c}, \tag{35}$$

and

$$n_n(x=a) \cong \left(\frac{\beta}{\beta_c}\right)^{1/2} \left(1 - \frac{\beta}{2\beta_c}\right). \tag{36}$$

Equation (29) is simplified to [62, 78]

$$\frac{\pi c}{(\beta\beta_c)^{1/2}} = N_T, \tag{37}$$

and equation (32) is simplified to

$$P = \varepsilon_T(T) n_0 c \left(\frac{\beta}{\beta_c}\right)^{1/2}. \tag{38}$$

4.2. Collisionless plasma

A free-fall model for the collisionless ions accounts for the finite temperature of the ion fluid that results from ionization at various locations [2, 15, 16, 72, 79]. For simplicity, however, we use here our cold fluid model presented above. In a collisionless plasma,

$$\frac{\beta_c}{\beta} \ll 1, \tag{39}$$

so that we write

$$\Gamma_n^2 = 4n_n(1-n_n), \quad M = \frac{\Gamma_n}{1+\sqrt{1-4\Gamma_n^2}}, \ \Gamma_{\max} = \frac{n_0 c}{2}. \tag{40}$$

The minimal plasma density is at the wall where $\Gamma_n = 1$. The dimensionless minimal plasma density is $n_n = 0.5$. Equation (29) is simplified in this case to [77]

$$\frac{(\pi-2)\,c}{\beta} = N_T, \tag{41}$$

while equation (32) becomes

$$P = \varepsilon_T(T)\frac{n_0 c}{2}. \tag{42}$$

5. Collisional plasma—neutral depletion due to electron pressure

We now analyze an unmagnetized plasma in which plasma and neutrals are collisional, and are coupled by ion–neutral collisions. Both planar geometry and cylindrical geometry are addressed here. Although neutral depletion in collisional plasma had already been calculated in early studies [23, 24], the analysis here follows [62, 72], to present certain specific results with analytical expressions that are derived for planar geometry. For the more common cylindrical geometry, numerical solutions are presented.

In the collisional plasma and collisional neutral gas, the pressure gradient of each is balanced by the drag force due to mutual ion–neutral collisions. The inertia terms of both ions and neutrals are neglected, as well as the momentum of the neutrals due to their drift velocity V (the first terms on the RHS of equations (2) and (6)). Neutrals are thermalized, and the neutral-gas pressure is taken as

$$p_N = NT_g, \tag{43}$$

where T_g is the gas temperature. Since neutrals experience ion–neutral collisions more than ionization events, neutral pumping is the source of neutral depletion.

The momentum equations for collisional plasma and neutral gas are reduced to

$$\frac{\mathrm{d}(nT)}{\mathrm{d}x} = -m\beta_c N\Gamma, \tag{44}$$

for the plasma and

$$\frac{\mathrm{d}(NT_g)}{\mathrm{d}x} = m\beta_c N\Gamma. \tag{45}$$

for the neutrals. The drag on the ions (neutrals) due to collisions with neutrals (ions) points inward (outward), is balanced by the gradient of the plasma (neutral) pressure that exerts an outward (inward) force. Equation (45) is an approximation of equation (17) when only the first term on the LHS and the second term on the RHS of the equation are retained, and the neutral pressure is expressed through equation (43).

We note that equations (44) and (45) also hold in a cylindrical geometry when x is replaced by r. Therefore, the following analysis holds for both planar and cylindrical geometries.

Adding the two equations (44) and (45), we obtain an equation that expresses a pressure balance between plasma and neutrals. The pressure balance is expressed as

$$p_r = NT_g + nT, \tag{46}$$

where p_r, the total pressure, is uniform. The total pressure is then $p_r = N_w T_{g,w}$, where $T_{g,w}$ is the neutral temperature at $x = \pm a$. We therefore write

$$NT_g + nT = N_w T_{g,w}. \tag{47}$$

Equations (46) and (47) are approximations of equations (10) and (12) for unmagnetized collisional plasma. In collisional plasma, $n_W \ll n_0$, and therefore even if $n_0 T$ is comparable to $N_W T_g$, the plasma pressure near the wall, $n_W T$, can be neglected relative to $N_W T_g$. Thus, in this collisional case, we make the diffusion approximation that $n(\ x = \pm a) = 0$.

In this case of pressure balance, we may write the expression for the neutral depletion, as was done in [81, 82], as

$$1 - D = (1 - D_e)\,(1 - D_{Tg})\,, \tag{48}$$

where D_e is the neutral depletion due to the electron pressure

$$D_e \equiv \frac{n_0 T}{N_w T_{g,w}}, \tag{49}$$

while D_{Tg} is the neutral depletion due to the neutral-gas heating,

$$D_{Tg} \equiv 1 - \frac{T_{g,W}}{T_g(0)}. \tag{50}$$

Here, $T_g(0)$ is the gas temperature at the central plane, $x = 0$. In this section we assume that T_g is uniform, so that

$$T_g(x) = T_g. \tag{51}$$

Therefore, neutral depletion discussed in this section is due to electron pressure. Neutral depletion due to gas heating is discussed in the next section.

In the analysis here β_c is assumed constant as in [62, 72]. Neutral depletion in the case that v is larger than the neutral thermal velocity, so that β_c is linearly proportional to v [9], is not presented here. This case of nonconstant β_c has also been addressed in [62], and then formulated in detail in [72].

5.1. Planar geometry

The continuity equations for the plasma and neutral gas, equations (1), (5) and (3), hold here as well as through all this paper for the planar geometry. Combining equations (1) and (44) with the explicit form of the neutral density, equation (46), we obtain a nonlinear diffusion equation for the normalized plasma pressure $p_i \equiv nT/\left(N_W T_g\right)$,

$$\frac{\mathrm{d}}{\mathrm{d}\xi}\left[\frac{1}{(1-p_i)}\frac{\mathrm{d}p_i}{\mathrm{d}\xi}\right] + \alpha_L\,(1-p_i)\,p_i = 0, \tag{52}$$

where $\xi \equiv x/a$, and

$$\alpha_L \equiv \frac{\beta_c \beta N_W^2 a^2}{c^2}, \tag{53}$$

a parameter that was defined slightly differently in [62]. In the case that $p_i \ll 1$, equation (52) is reduced to the familiar linear diffusion equation [1]. With equations (53) and (37), we can also write

$$\alpha_L^{1/2} = \pi \frac{N_W a}{N_T}, \tag{54}$$

showing that in the weakly-ionized case (when $N_T = 2N_W a$) $\alpha_L^{1/2} = \pi/2$. We use the auxilliary variable θ, so that $\Gamma_n = \sin\theta$ and $n_n = \cos\theta$, to transform equation (52) into

$$\alpha_L^{1/2}\xi = \int_0^{\theta} \frac{\mathrm{d}\theta'}{1 - D_e\cos\theta'}. \tag{55}$$

The solvability condition is

$$\alpha_L^{1/2} = \int_0^{\pi/2} \frac{\mathrm{d}\theta}{1 - D_e\cos\theta}, \tag{56}$$

and it relates the neutral depletion due to electron pressure D_e and the parameter $\alpha_L^{1/2}$. We derive further analytical expressions. Integrating equation (56) and imposing $p_i(x = \pm a) = 0$, we obtain the solvability condition as [62]

$$\alpha_L^{1/2}\cos\theta_0 = \theta_0 + \frac{\pi}{2}, \tag{57}$$

a condition that relates the parameter $\alpha_L^{1/2}$ algebraically to

$$\theta_0 \equiv \arcsin\frac{n_0 T}{N_W T_g} = \arcsin D_e. \tag{58}$$

The algebraic plasma balance equation, equation (57), can be cast in the form of Kepler's equation [137]. Interestingly, such an equation has also been used to describe the dynamics of a quantum kicked rotor [138].

We note that in this case of pressure balance with uniform gas temperature, the neutral depletion satisfies

$$D = D_e = \frac{n_0 T}{N_W T_g} = \sin\theta_0, \tag{59}$$

so that, in fact, equation (57) relates the neutral depletion D to the parameter $\alpha_L^{1/2}$. The relation is written equivalently as

$$D = -\cos\left[\alpha_L^{1/2}\sqrt{1 - D^2}\right]. \tag{60}$$

The profile of the plasma density is expressed in an implicit form as

$$\frac{n_n - \sin\theta_0}{\Gamma_n\cos\theta_0} = \cot\left[\left(\theta_0 + \frac{\pi}{2}\right)\xi\right], \tag{61}$$

where Γ_n and n_n are defined in equations (27) and (34). Equations (57) and (61) are generalizations of the weakly-ionized uniform neutral density case to include neutral depletion. When neutral depletion is small, when $\theta_0 \ll \pi/2$, these relations yield $\alpha_L = (\pi/2)^2$, $\theta = (\pi/2)\,(1 - \xi)$ and $n_n = \cos\left[(\pi/2)\,\xi\right]$, the specified value of α_L then determines

the electron temperature, recovering the case of uniform neutral density.

The implicit expression, equation (61), can be modified so as to provide an explicit expression for the plasma density profile,

$$n_n = \frac{D\sin^2\left[\left(\arcsin D + \frac{\pi}{2}\right)\xi\right] + \left(1-D^2\right)\cos\left[\left(\arcsin D + \frac{\pi}{2}\right)\xi\right]}{1 - D^2\cos^2\left[\left(\arcsin D + \frac{\pi}{2}\right)\xi\right]}. \tag{62}$$

Raimbault *et al*. [72] solved the collisional case in an equivalent way, and derived a different—perhaps more convenient—explicit expression for the plasma density, which, in the notation used here, is

$$n_n = \frac{\tan^2\left(\frac{\arcsin D}{2} + \frac{\pi}{4}\right) - \tan^2\left[\left(\frac{\arcsin D}{2} + \frac{\pi}{4}\right)\xi\right]}{\tan^2\left(\frac{\arcsin D}{2} + \frac{\pi}{4}\right) + \tan^2\left[\left(\frac{\arcsin D}{2} + \frac{\pi}{4}\right)\xi\right]}. \tag{63}$$

The neutral density profile is expressed in terms of the plasma density and the neutral depletion as

$$\frac{N}{N_W} = 1 - Dn_n. \tag{64}$$

Equation (57) relates the plasma maximal density (through θ_0) and the electron temperature (through $\alpha_L^{1/2}$) to the discharge parameters. If the total number of particles per unit area, N_T, is specified, the electron temperature T is determined through equation (37). However, often N_T is not specified experimentally. In the nonlinear problem of modified neutral density, the particle balance equation is usually not sufficient to determine the electron temperature. We may use power balance in addition to particle balance to solve simultaneously for the electron temperature and density. For determining power balance, we use equation (38).

The equations above allow us to find the plasma and neutral variables if sufficient control parameters are known. Let us assume that the atomic rates β and β_c and ε_T are known as functions of T, and a is specified. If the total pressure p_r, the (assumed uniform) gas temperature T_g and the power per unit area P are specified, we can use equations (60) and (38) to find n_0 (through D) and T, using $N_W = p_r/T_g$. The density profile is then calculated. If the total number of neutrals N_T, T_g and P are given, we use equation (37) to find T, and then equation (38) to find n_0. Equation (60) is then used to calculate D and finally, through equation (59), N_W is found.

We present here numerical examples taken from [62]. The discharge gas is argon at room temperature, the pressure prior to the discharge ignition is 10mTorr, and $a = 5$ cm. Figure 1 shows the plasma and neutral density profiles, characteristic of neutral depletion. The calculations shown are for low power and for high power—each for two cases, one of a fixed total number of neutrals (per unit area), N_T, and a second of a fixed neutral density at the wall, N_W. When the power is low, the neutral density almost does not vary with ξ, and the plasma density has the familiar $\cos\left[(\pi/2)\,\xi\right]$ form. When the power is high, the neutral and plasma densities are uniform across most of the discharge volume and drop sharply to zero (plasma) or peak sharply to a high density (neutrals) near the wall, similarly to what was found in measurements ([48], for example). Note that in the first case, the fixed total number

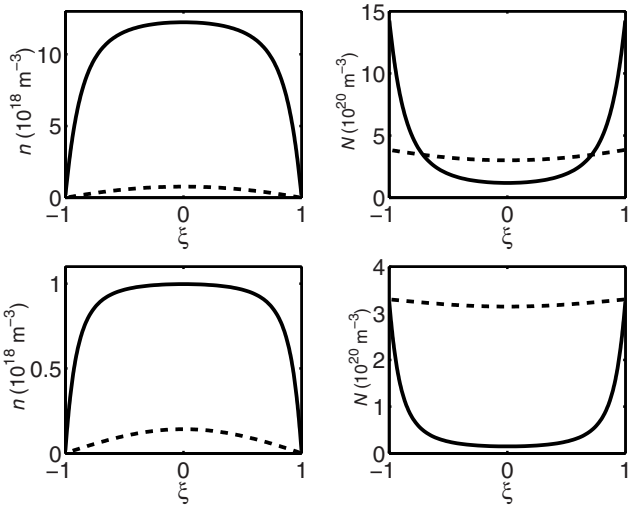

Figure 1. Collisional unmagnetized plasma, planar geometry. Plasma and neutral density profiles, fixed total neutrals number—top ($P = 33$ kW m^{-2} and 509 kW m^{-2}), fixed neutral density at the boundary—bottom ($P = 3$ kW m^{-2} and 121 kW m^{-2}). Reprinted figure with permission from [62], Copyright 2005 by the American Physical Society.

of particles results in an *increase* of the total pressure with power. The increase of the total pressure, $N_W T_g$, is expressed in figures 1(a) and (b) at the discharge center by a large plasma pressure and near the wall by an increased neutral pressure.

The dependencies of the discharge parameters on power are shown in figure 2 for fixed N_W (and, therefore, a fixed total pressure $N_W T_g$). Here, a surprising effect of neutral depletion was demonstrated. As is shown in figure 2, the increase of power for a fixed total pressure is followed by an increase of plasma pressure at the expense of the neutral pressure. The decrease of N_T (the total number of neutrals per unit area, not shown in figure 2) is followed by an increase of the electron temperature T (according to equation (37)). Since the energy ε_T is a decreasing function of T, it follows from equation (25) that the increase of the electron temperature T with power results in an increase of the plasma flux $\Gamma_{\max}$ with power—an increase that is faster than linear. What was unexpected was that, despite the fast increase of $\Gamma_{\max}$ with power, i.e. the fast increase of plasma production with power, the plasma density does not increase faster when the power is increased. Moreover, the behavior is nonmonotonic, and above a certain power, the plasma density *decreases* with the power *increase*. As is shown in the figure, this is true for both $n(0)$ and the total number of plasma particles, $n_T \equiv \int_{-a}^{a} \mathrm{d}x n = (T_g/T)\,(2N_w a - N_T)$ (following equations (46) and (37)). Formally, this dependence follows the relation $n_0 = (\Gamma_{\max}/c)\,(\beta_c/\beta)^{1/2}$ (equation (34)). If $\Gamma_{\max}$ increases while T is constant or increases slowly, n_0 increases as well. However, when the increase of $\Gamma_{\max}$ is followed by a fast increase of β due to the increase of T, n_0 decreases with $\Gamma_{\max}$. The decrease of plasma density with power exhibited in figure 2 is a result of deconfinement of the plasma caused by neutral depletion. The drag of the neutrals on the ions decreases when the neutrals are depleted. Thus, even though *more* ions are produced, they escape the volume

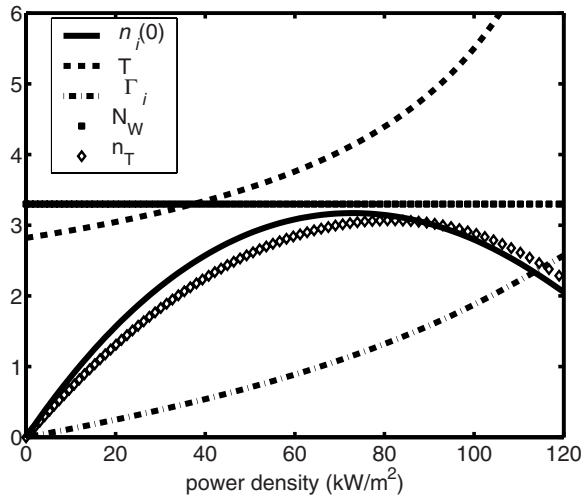

Figure 2. Collisional unmagnetized plasma, planar geometry. Fixed neutral density at the boundary: $N_W(10^{20}\ \mathrm{m}^{-3})$, T (eV), $\Gamma_i(5\times10^{21}\ \mathrm{m}^{-2}\ \mathrm{s}^{-1})$, $n_i(0)\ (5\times10^{17}\ \mathrm{m}^{-3})$, $n_T\ (2\times10^{16}\ \mathrm{m}^{-2})$. Γ_i and $n_i(0)$ in the figure were denoted in this paper as $\Gamma_{\max}$ and n_0. Reprinted figure with permission from [62], Copyright 2005 by the American Physical Society.

faster, and therefore their density is *lower*. A nonmonotonic dependence of the plasma density on the wave power has been indeed measured by Denning *et al* [83].

5.2. Cylindrical geometry

When cylindrical geometry is considered, the continuity equation becomes

$$\frac{1}{r}\frac{\partial\left(r\Gamma\right)}{\partial r}=\beta Nn, \tag{65}$$

where we have also used equation (3). Equation (65), together with equations (44) and (47) are the governing equations. The plasma particle flux density Γ is in the positive radial direction. For cylindrical geometry, there is no particular advantage in using dimensionless quantities. It is also noted that simple relations between Γ and n such as in equation (34), that were derived for planar geometry, do not exist in cylindrical geometry.

Figure 3 presents the dependencies on the plasma particle flux density at the wall Γ_W of the discharge parameters of a cylindrical plasma. Note that in cylindrical geometry, Γ at the wall is denoted as Γ_W and not as $\Gamma_{\max}$—since, because of the geometry, Γ is not maximal at the wall ($2\pi r\Gamma$ is maximal at the wall). Figure 3 for the dependence on Γ_W in cylindrical geometry is equivalent to figure 2 for the dependence on power in a planar geometry. The dependence is nonmonotonic also in cylindrical plasma. The plasma maximal density n_0 (denoted as n in the figure) and the total number of plasma particles for unit length $n_T\equiv\int_0^a 2\pi rndr$ increase with the plasma particle flux density Γ_W for low Γ_W, but for a high Γ_W both n_0 and n_T decrease with Γ_W. The reason for that nonmonotonic dependence is the same as in the planar geometry. The plasma residence time decreases with neutral depletion at higher Γ_W so that the plasma density is lower, even though more plasma is produced (higher Γ_W).

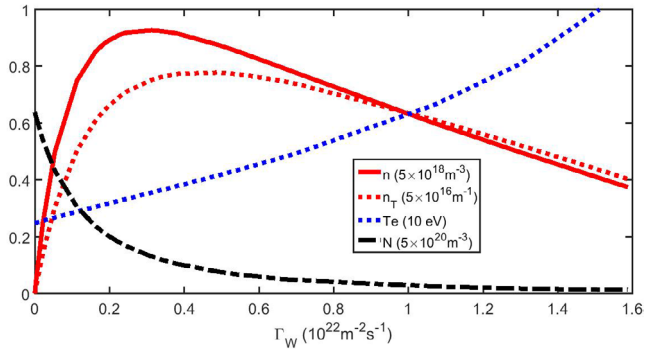

Figure 3. Collisional unmagnetized plasma, cylindrical geometry, $a=0.1$ m, $p_r=1.33$ Pa. Maximal plasma density n_0 (denoted as n), total plasma density per unit length n_T, minimal neutrals density N_0 (denoted as N), and electron temperature versus Γ_W. Nonmonotonic dependence of n and n_T as in planar geometry.

6. Collisional plasma—neutral depletion due to gas heating

In this section, neutral depletion due to gas heating is analyzed. The change of neutral temperature for collisional neutrals was analyzed employing a hydrodynamic formalism by Valentini *et al*, in which the hierarchy of fluid equations was closed by relating the heat flux tensor to the pressure tensor [25, 26]. Here, we use a simpler model for estimating the gas heating and the associated neutral depletion. The heating of neutral gas by collisions with electrons and with ions is balanced by heat conduction towards the walls, as was assumed in [55, 74, 78]. The analysis here mostly follows [78].

Neutral atoms can gain kinetic energy when they are generated through recombination at the wall. The recombining ions carry a high kinetic energy upon hitting the wall—an energy they acquire while they move towards the wall across the sheath. A re-emitted neutral atom can carry part of the kinetic energy of the impinging ion, according to the accommodation coefficient, which causes an effective gas heating [20, 21, 57, 66]. In this paper, we neglect this source of gas heating. Volume heating through collisions of neutrals with the higher-temperature electrons and ions is considered the dominant source of gas heating.

The rate of gas heating per unit volume $Q(z)$ is composed of several sources [74, 78], based on [10, 139]. As in [78], we retain in the analysis two sources,

$$Q(z)=nNq+nNm\beta_c v^2. \tag{66}$$

In [78], Q was denoted as p_N. The first term on the RHS is due to electron–neutral collisions, while the second term is due to ion–neutral collisions, the work done by the ion flow colliding with neutrals. In atomic-gas discharges we take into account electron–neutral elastic collisions,

$$q=\beta_{em}T, \tag{67}$$

where $\beta_{em}\equiv 3\left(m_e/m\right)\beta_e$, β_e is the electron–neutral momentum transfer rate constant. For example, using the expression of β_e [10], we obtain that for argon, $\beta_{em}\cong 5\times10^{-18}\ \mathrm{m}^3\ \mathrm{s}^{-1}$. In equation (67) we approximated $T-T_g=T$, as $T\gg T_g$.

Often, energy released through molecular dissociation by electron impact is a major source of gas heating. If there is a

minority of molecular gas within a gas that is mostly atomic gas, the energy of Franck–Condon dissociated atoms is transferred to the atomic gas through collisions. The rate of heating of the atomic gas in this process is $Q_{\rm diss} = NN_2 \langle \sigma v \rangle_2 \Delta E_{\rm diss}$, where N and N_2 are the respective densities of the atomic gas and of the dissociated hot atoms, $\langle \sigma v \rangle_2$ is the collision rate constant between the majority atoms and the dissociated hot atoms, and $\Delta E_{\rm diss}$ is the energy of Franck–Condon dissociated atoms. We assume that we can write $N_2 = n \langle \sigma v \rangle_{\rm diss} N_m \tau$, where $\langle \sigma v \rangle_{\rm diss}$ is the dissociation rate constant, N_m is the density of the molecular gas, and τ is the residence time in the discharge of the dissociated hot atoms. In that case, the rate of heating of the atomic gas due to the molecular dissociation can be expressed by the first term on the RHS of equation (66), while the rate constant is written as

$$q = q_{\rm diss} = N_m \langle \sigma v \rangle_2 \langle \sigma v \rangle_{\rm diss} \Delta E_{\rm diss} \tau. \tag{68}$$

With these simplifying assumptions ($q_{\rm diss}$ taken as uniform), the case that was simulated by Shimada *et al* [80] can also be analyzed approximately within the present formalism. When the chemistry becomes more complicated, a more detailed description might be needed [55, 91, 92].

When the mean free path for ion–neutral collisions is smaller than the system size, the ion velocity is inversely proportional to N. Therefore, the heating by electrons should be dominant at high neutral density, while the heating by ions should be dominant at a lower neutral density.

As we noted in section 2, in the diffusion approximation of the collisional case ($\beta \ll \beta_c$), in which the ion velocity v is infinite at the walls, the heating rate per unit volume is also infinite at the walls. As also explained in section 2, whenever finite values for the ion velocity and for the heating rate are needed in order to resolve a non-physical singularity, we may take the values at the wall as the values that correspond to $M = 1$ (equation (34)). The velocity is then the Bohm velocity, $v = c$, and the heating is finite.

We assume that the evolution of the neutral-gas temperature is governed by the following energy equation

$$\vec{\nabla} \cdot \left[K(T_g) \vec{\nabla} T_g \right] = -Q = -nN \left(q + m\beta_c v^2 \right), \tag{69}$$

as was described in [74, 78] based on [10, 139]. Here $K(T_g)$ is the coefficient of heat conductivity.

A numerical solution of equation (69) for a slab geometry is presented in figure 4. The profile of the neutral temperature, $\Delta T_g / \Delta T_{g,\max}$, is shown for two cases. In one case, the heating is by electrons only (the first term on the RHS of equation (69)) and in the second case the heating is by ions only (the second term on the RHS of the equation). The calculation was done for a weakly-ionized plasma, so that N is assumed uniform, $n \sim \cos\left[(\pi/2)\,\xi\right]$ and $v \sim \tan\left[(\pi/2)\,\xi\right]$. It is also assumed that q and K are uniform. It is seen in the figure that the gas temperature profile is flatter near the discharge center when the heating is by ion–neutral collisions—a heating which is larger near the wall, where the ion velocity v is larger.

In [78], gas heating by both electrons and ions is analyzed. In the following analysis here, we retain the gas heating by electrons only, the first term on the RHS of equation (69).

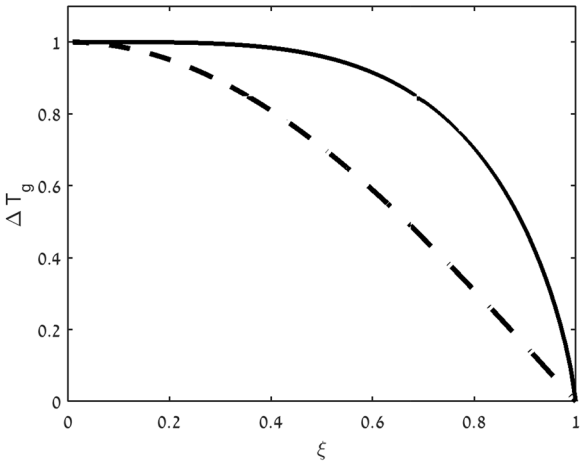

Figure 4. Collisional unmagnetized plasma, planar geometry. Neutrals heating in a weakly-ionized plasma by electron–neutral collisions (dashed line) and by ion–neutral collisions (solid line). Shown is $\Delta T_g / \Delta T_{g,\max}$ for $0 \leqslant \xi \leqslant 1$ only. The temperature profile is flatter near the discharge center when the heating is by ion–neutral collisions, a heating which is larger near the wall.

Thus $\vec{\nabla} \cdot \left[K(T_g) \vec{\nabla} T_g \right] = -Q = -qnN$. Writing the continuity equation as $\vec{\nabla} \cdot \vec{\Gamma} = \beta N n$, we note the similarity between plasma particle flux density $\vec{\Gamma}$ and heat flux density $K(T_g) \vec{\nabla} T_g$. As β and q are assumed uniform, we obtain that $K(T_g) \vec{\nabla} T_g + (q/\beta) \vec{\Gamma}$ is divergence free—and in fact, for the simple 1D, either planar or cylindrical geometry,

$$K(T_g) \vec{\nabla} T_g + (q/\beta) \vec{\Gamma} = 0. \tag{70}$$

Combining equation (70) with equation (44) and equation (47), we derive the relation $(\beta\beta_c m/q) \left(\partial \left(\int \left[K\left(T_g'\right) / T_g' \right] \mathrm{d}T_g' \right) / \partial \left(D_e n_n \right) \right) = \left(1 - D_e n_n\right)^{-1}$. This relation results in

$$\frac{\beta\beta_c m}{q} \int_{T_{g,W}}^{T_g} \frac{K\left(T_g'\right)}{T_g'} \mathrm{d}T_g' = -\ln\left(1 - D_e n_n\right). \tag{71}$$

The last two expressions hold for both planar and cylindrical geometries. It is now assumed for simplicity that

$$K(T_g) = K = \text{const.} \tag{72}$$

With these assumptions, equation (71) is solved for T_g

$$T_g = \frac{T_{g,w}}{\left(1 - D_e n_n\right)^{1/K_e}}, \tag{73}$$

where the normalized heat conductivity is

$$K_e \equiv \frac{K\beta\beta_c m}{q}. \tag{74}$$

The neutral depletion due to gas heating (equation (50)) is

$$D_{Tg} = 1 - \left(1 - D_e\right)^{1/K_e}. \tag{75}$$

The maximal gas temperature is

$$T_g(0) = \frac{T_{g,w}}{\left(1 - D_e\right)^{1/K_e}}. \tag{76}$$

We use equation (48) to express D, the neutral depletion due to both D_e, the electric pressure, and D_{Tg}, gas heating, through D_e only, as

$$D = 1 - (1 - D_e)^{1+1/K_e}. \tag{77}$$

Equivalently, we express the neutral density as

$$N = \frac{p_r}{T_g}(1 - D_e n_n) = N_W (1 - D_e n_n)^{1+1/K_e}. \tag{78}$$

The neutral density and temperature are related through

$$T_{gn} \equiv \frac{T_g}{T_{g,W}} = \left(\frac{N}{N_W}\right)^{1+K_e}. \tag{79}$$

The neutral temperature has been expressed through the algebraic expression, equation (73). These relations hold for both planar and cylindrical geometries. The analysis of neutral depletion with gas heating is first made for planar geometry where analytical expressions are derived. Then, neutral depletion with gas heating is solved numerically for cylindrical geometry. The model presented here should be useful in guiding the analysis of measurements of gas heating, as described in section 2—an analysis that often requires, in addition, a numerical modeling and a more detailed chemistry description.

6.1. Planar geometry

In a planar geometry, the continuity equation becomes

$$\frac{\mathrm{d}\Gamma_n}{\mathrm{d}\xi} = \alpha_L^{1/2} (1 - D_e n_n)^{1+1/K_e} n_n, \tag{80}$$

where $\alpha_L^{1/2}$ is defined in equation (53) and $N_W = p_r/T_{g,w}$, and $\xi = x/a$, as before. For a planar geometry, Γ_n and n_n are related through equation (34). As above, we use the auxiliary variable θ, so that $\Gamma_n = \sin\theta$ and $n_n = \cos\theta$, to express the density profile as

$$\alpha_L^{1/2}\xi = \int_0^\theta \frac{\mathrm{d}\theta'}{(1 - D_e\cos\theta')^{1+1/K_e}}, \tag{81}$$

and to write a solvability condition:

$$\alpha_L^{1/2} = \int_0^{\pi/2} \frac{\mathrm{d}\theta}{(1 - D_e\cos\theta)^{1+1/K_e}}. \tag{82}$$

Equations (81) and (82) generalize equations (55) and (56) to finite gas heating. As expected, in the case of a small plasma pressure, $D_e \ll 1$, equations (81) and (82) are reduced to Schottky's case [1]: $\alpha_L^{1/2} = \pi/2$.

The parameters in the last two equations are D_e, $\alpha_L^{1/2}$, and K_e, but usually the unknowns are n_0 and T. In addition to particle balance—equation (82)—we may use power balance—equation (38)—to find n_0 and T, which determine the values of D_e, $\alpha_L^{1/2}$, and K_e.

When the normalized heat conductivity is small, $K_e \ll 1$, we can employ Laplace's method [140] to obtain an asymptotic form of the integral in equation (82). At that limit, the integral becomes [78]

$$\alpha_L^{1/2} = \left(\frac{\pi K_e}{2D_e}\right)^{1/2} \frac{1}{(1 - D_e)^{1/2+1/K_e}}. \tag{83}$$

The numerical examples—figures 5 and 6—are taken from [78]. We calculate the pressure and density profiles of plasma and neutrals for four different values of the heat conductivity. In all four cases, the total number of neutrals per unit area, N_T, the deposited power P, and the wall temperature $T_{g,w}$ are specified and are constant. Since the total number of neutrals is fixed, the electron temperature T is also fixed (according to equation (37)). The total power is fixed and therefore the maximal plasma density n_0 is also fixed, according to equation (38). For different values of K_e, the total pressure p_r and the profile of the neutral-gas temperature $T_g(x)$ are different. If, for the same number of neutrals and the same deposited power, K_e is smaller, D_e $(= n_0 T/N_W T_{g,W})$ should be smaller and $\alpha_L^{1/2}$ should be larger—both by the same numerical factor, corresponding to a larger N_W. We present calculations for four cases, where $K_e = \infty, 1, 1/9$, and $1/49$, and $D_e = 0.9, 0.7025, 0.286$, and 0.089. We then determine the values of $\alpha_L^{1/2}$ through the integral in equation (82).

Figure 5 presents for each of the four cases the normalized plasma pressure $nT/p_{r,1}$, where $p_{r,1} = N_{W1} T_{g,W}$ is the total pressure and $N_{W,1}$ is the neutral density at the wall, when the heat conductivity is infinite, $K_e = \infty$. The normalized neutral pressure $NT/p_{r,1}$ is also presented in figure 5. Figure 6 shows the normalized neutral-gas temperature $T_g/T_{g,w}$ and density $NT_{g,w}/p_{r,1}$ for the four cases. As is expected, it is seen in the figures that a lower K_e results in a higher T_g, a higher neutral depletion D, and a higher total pressure p_r. Even though the plasma pressure becomes smaller relative to the total pressure, so that D_e becomes smaller, the larger neutral heating results in a larger neutral depletion D. An increase of D with a decrease of D_e for a pressure increase was indeed measured by O'Connell *et al* [81, 82], but not for a constant number of neutrals.

6.2. Cylindrical geometry

In cylindrical geometry, the governing equations are solved here numerically. These are the continuity equation in cylindrical geometry, equation (65), and the plasma momentum equation, equation (44), together with the expression for N when the gas is heated, equation (78). Once the equations are solved and $n(r)$ is calculated, the neutral temperature $T_g(r)$ is found from equation (73).

Figures 7 and 8 show the discharge parameters as a function of Γ_W for an argon plasma in a cylindrical tube of radius $a = 0.1$ m and pressure near the wall $p_r = 13.3$ Pa (100 mTorr). The heating is due to electron–neutral collisions. The heat conductivity of argon is taken as constant, with a characteristic value [86] of $K = 1.5 \times 10^{21}$ m^{-1} s^{-1}.

Two figures, 7 and 8, show the dependencies on Γ_W in order to enable inspection of the behavior for small values of the plasma flux density Γ_W. It is seen in figure 7 that for

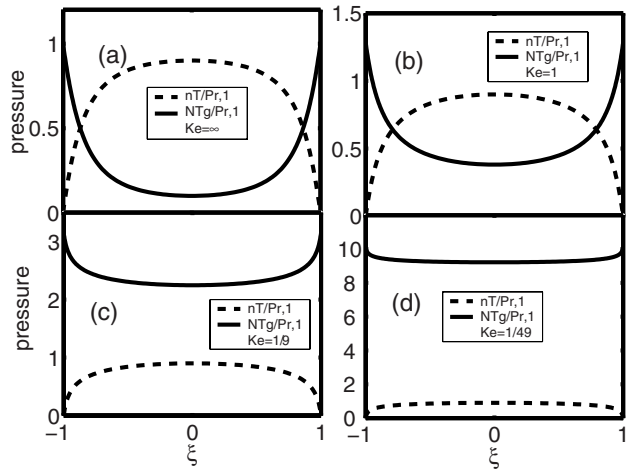

Figure 5. Collisional unmagnetized plasma, planar geometry. Normalized plasma and neutral pressures for four different coefficients of normalized heat conductivity, K_e. The resulting normalized total pressure $N_W T_{g,W}/N_{W,1}T_{g,W} = N_W/N_{W,1}$ is: (a) 1, (b) 1.281, (c) 3.147, (d) 10.112. Reproduced from [78]. © IOP Publishing Ltd. All rights reserved.

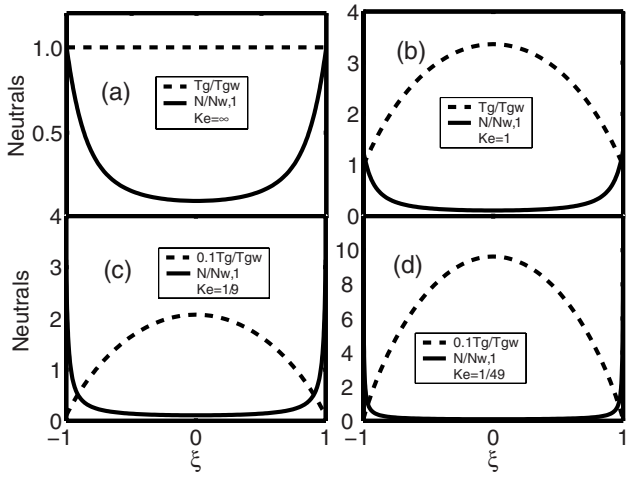

Figure 6. Collisional unmagnetized plasma, planar geometry. Normalized neutral-gas density and temperature for four different coefficients of normalized heat conductivity, K_e, as in figure 3. The resulting maximal normalized neutral density $N_W/N_{W,1}$ equals the normalized total pressure $N_W T_{g,W}/N_{W,1}T_{g,W}$:(a) 1, (b) 1.281, (c) 3.147, (d) 10.112. The maximal normalized neutral temperature $T_g(\xi = 0)/T_{g,w}$ is (a) 1, (b) 3.3613, (c) 20.73, (d) 96.29. The neutral depletion D is: (a) 0.9, (b) 0.9115, (c) 0.965 52, (d) 0.990 54. Note that in (c) and in (d) $0.1T_g/T_{g,w}$ is presented. Reproduced from [78]. © IOP Publishing Ltd. All rights reserved.

a small Γ_W there is a substantial gas heating that results in neutral depletion. This is despite the plasma pressure being small at this stage. As is seen in figure 8, for a larger Γ_W, the plasma pressure is comparable to neutral pressure. Then plasma (electron) pressure is the source of neutral depletion. It is also seen in figure 8 that, in addition to the plasma density (n_0 and n_T), the variation of $T_{gno}(= T_{gn}(x = 0))$ is also not monotonic. The neutral temperature, T_{gn0}, first increases, but then decreases with Γ_W. This is a result of K_e becoming large as T increases. The figures exhibit clearly the different regimes in which either D_e or D_{Tg} is dominant.

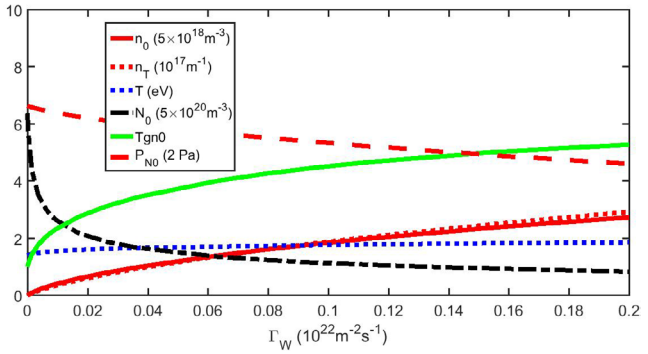

Figure 7. Neutral gas heating in collisional unmagnetized plasma, cylindrical geometry, $a = 0.1$ m, $p_r = 13.3$ Pa. The neutrals temperature T_{gn0} (at $r = 0$) is normalized to 300 K. The neutrals pressure at the discharge center P_{N0} (at $r = 0$) hardly changes while N_0 (also at $r = 0$) decreases and T_{gn0} increases.

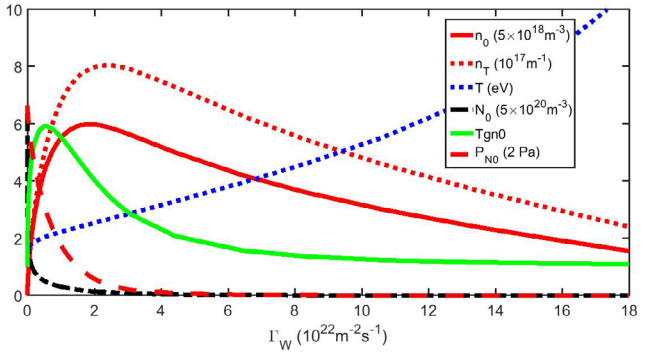

Figure 8. Neutral gas heating in collisional unmagnetized plasma, cylindrical geometry. The same calculation as in figure 7 on a larger range of Γ_W. It is seen that n_0, n_T and also T_{gn0} are not monotonic with Γ_W.

7. Collisionless unthermalized neutrals—ion pumping

In this section, we assume that the neutrals are collisionless, so that they do not collide with ions, and are coupled to the plasma only through volume ionization and wall recombination. Moreover, we assume that the neutrals move ballistically, without colliding between themselves, so that they are not thermalized. We also assume that the plasma ions are collisionless.

A discharge in which both neutrals and ions are collisionless, and are coupled through ionization, has been studied in various degrees of detail. As described in the Introduction, in a 1964 paper, Caruso and Cavaliere assumed two monoenergetic neutral beams moving in opposite directions in a planar geometry [15]. Since ions are born through ionization at different locations, they were described by a free-fall model where their pressure is not zero. The model has been extended in 1971 by Valentini [16] and by Torven [17] to also address a cylindrical geometry. Also in 1971, Stangeby and Allen calculated, in [18], the neutral depletion of ballistic neutrals in a cylindrical geometry, while plasma was assumed to be an ionizing uniform background. In 1976, Valentini used the Boltzmann equation to derive equations for the moments of the velocity distributions of both neutrals and ions in planar and cylindrical

geometries [22]. He then closed the hierarchy of fluid equations by relating the heat flux tensor to the pressure tensor [25, 26]. Valentini showed that both pressure and temperature become anisotropic under these conditions. The initial velocity of the ions born through ionization was also taken into account. Due to this initial velocity, an ion born through ionization could initially move toward the center of the discharge against the electric force, then being reflected back towards the wall [23, 24]. The effect of this initial ion velocity becomes small if the neutral temperature is smaller relative to the kinetic energy that ions can acquire through their fall across the potential drop. Neutrals have also been assumed to move ballistically in certain later studies [48, 60, 73, 77, 79].

We treat the neutrals here similarly to what was originally done in [15]. The neutrals move ballistically between the walls in a planar geometry. We will initially allow a general velocity distribution function for the neutrals, and then write the solution for two counter-streaming monoenergetic beams. The plasma could be treated with a free-fall picture, as was also used in later publications (for example, in [79]). However, for simplicity the plasma ions are treated as a cold fluid, as was described in section 4. This is definitely an approximation only, since being born in different locations, not all ions have the same velocity at a particular location. This simplified picture demonstrates, though, some of the features of neutral depletion in a collisionless plasma—as well as features of the pressure moment of the neutrals.

Collisionless neutrals that move ballistically are depleted at the discharge center as a result of ionization within the plasma—a process we term 'ion pumping'. Neutral depletion with ballistic neutrals has been examined theoretically often over the years. The analysis of neutral depletion with ballistic neutrals presented here follows [15, 16, 22, 77, 79]. It is shown here that the discharge center is the location of the lowest neutral density but the highest neutral pressure. The total pressure of the neutrals (which includes the inertia contribution) is shown to be lowest at the discharge center. Analytical expressions for the neutral variables are presented for a simple case.

The fluid equations for the neutrals are reduced in the case of collisionless neutrals to

$$\frac{\mathrm{d}\Gamma_N}{\mathrm{d}x} = -\beta N n, \quad \frac{\mathrm{d}\left(mNV^2 + p_N\right)}{\mathrm{d}x} = -m\beta N n V. \tag{84}$$

The neutral pressure p_N for ballistic neutrals will be derived here through a kinetic analysis.

The neutral-gas distribution function, $f_N(v,x)$, is obtained by solving the steady-state Boltzmann equation,

$$\frac{\mathrm{d}\left(vf_N\right)}{\mathrm{d}x} = -\beta n f_N, \tag{85}$$

and is found to be

$$f_N(v,x) = f_N(v,-a)\exp\left[-\frac{\beta}{v}\int_{-a}^{x} n(x')\,\mathrm{d}x'\right]. \tag{86}$$

We showed in [77] that neutrals of a distribution function described by equation (86) are depleted for every $f_N(v,-a)$ (this had already been shown in previous studies [15–17]). Thus, collisionless neutrals that move ballistically between the walls will always have a lower density away from the walls, independent of their distribution function at the wall. In contrast, as we have already noted, if a neutral gas is both collisionless and thermalized, it should experience repletion [72, 79, 89]—the density maximum of the neutrals being at the center of the discharge chamber, away from the walls. Repletion is discussed in section 9, where the possible existence of neutrals that are both collisionless and thermalized is challenged.

We apply the formalism to the simple case that the neutral gas is composed of two monoenergetic counter-streaming beams [15, 16, 22, 77, 79]. The neutral-gas distribution function is then

$$f_N(v,x) = \frac{\Gamma_1(x)}{v_a}\delta(v-v_a) + \frac{\Gamma_2(x)}{v_a}\delta(v+v_a). \tag{87}$$

The neutral density, particle flux-density and velocity are

$$N(x) = \frac{\Gamma_1(x)+\Gamma_2(z)}{v_a},\ \Gamma_N(x) = \Gamma_1(x) - \Gamma_2(x),\ V(x) = v_a\frac{\Gamma_1(x)-\Gamma_2(x)}{\Gamma_1(x)+\Gamma_2(x)}, \tag{88}$$

while the neutral pressure is

$$p_N(x) = \int_{-\infty}^{\infty}\mathrm{d}v f_N(v,x)\,m(v-V)^2 = \frac{4m\Gamma_1(x)\Gamma_2(x)}{N(x)}. \tag{89}$$

From the continuity equations for the two separate beams

$$\frac{\mathrm{d}\Gamma_1}{\mathrm{d}x} = -\beta n\frac{\Gamma_1}{v_a}, \quad \frac{\mathrm{d}\Gamma_2}{\mathrm{d}x} = \beta n\frac{\Gamma_2}{v_a}, \tag{90}$$

it follows that

$$\Gamma_1(x)\Gamma_2(x) = \frac{N_0^2 v_a^2}{4}, \tag{91}$$

where, as noted above, N_0 is the lowest value of the neutral density, attained at $x = 0$. The pressure is therefore

$$p_N(x) = \frac{mN_0^2 v_a^2}{N(x)}. \tag{92}$$

The neutral pressure turns out to be inversely proportional to the neutral density.

A straightforward analysis provides further relations. Such is the relation between the neutral particle flux density and the neutral density,

$$N = \frac{\sqrt{\Gamma_N^2(z) + N_0^2 v_a^2}}{v_a}. \tag{93}$$

Following equation (90), we can express the neutral-gas variables in terms of the plasma density distribution,

$$\Gamma_N = \frac{N_W v_a}{\cosh\left(\frac{\beta}{v_a}\frac{n_T}{2}\right)}\sinh\left(-\frac{\beta}{v_a}\int_0^x n(x')\,\mathrm{d}x'\right), \tag{94}$$

$$N = \frac{N_W}{\cosh\left(\frac{\beta}{v_a}\frac{n_T}{2}\right)}\cosh\left(-\frac{\beta}{v_a}\int_0^x n(x')\,\mathrm{d}x'\right), \tag{95}$$

and

$$V = v_a\tanh\left(-\frac{\beta}{v_a}\int_0^x n(x')\,\mathrm{d}x'\right). \tag{96}$$

Here,

$$n_T \equiv \int_{-a}^{a} n(x)\mathrm{d}x \tag{97}$$

is the total number of plasma particles per unit area.

The neutral variables Γ_N, N, and V satisfy equation (17) when the second term on the RHS, that express neutral collisions with ions, is neglected. The equation then reads

$$\left(-\frac{N_0^2}{N^2}v_a^2 - V^2\right)\frac{\mathrm{d}N}{\mathrm{d}x} = \beta n \Gamma_N. \tag{98}$$

We have substituted into the equation the expression for the neutral pressure, equation (92), and the expression for the ionization rate, equation (3). Since $\Gamma_N < 0$, the derivative of the neutral density is negative, $\mathrm{d}N/\mathrm{d}x < 0$, so that there is neutral depletion. We also note that the total neutral pressure is not uniform. It is easily verified that the total neutral pressure, $p_{NT} \equiv mNV^2 + p_N$, satisfies

$$p_{NT} = mNV^2 + p_N = mNv_a^2. \tag{99}$$

The total neutral pressure p_{NT} is linearly proportional to the neutral density, and is lowest at the center of the discharge. The ionization modifies the momentum of the neutrals. As mentioned above, each term on the RHS of equation (6) is positive; here, only the first term on the RHS of equation (6) is nonzero, and this term causes the total neutral pressure to increase from the discharge center towards the wall. This is in contrast to the decrease of p_N from the discharge center towards the wall.

From the expression for the neutras density we find that

$$N_0 = \frac{N_W}{\cosh\left(\frac{\beta}{v_a}\frac{n_T}{2}\right)}, \tag{100}$$

so that the neutral depletion is

$$D \equiv 1 - \frac{N_0}{N_W} = 1 - \frac{1}{\cosh\left(\frac{\beta}{v_a}\frac{n_T}{2}\right)}. \tag{101}$$

Similar expressions have been presented in [16, 21].

Following equation (94), we express the neutral particle flux density at the wall as

$$\Gamma_N(x=a) = N_W v_a \tanh\left(-\frac{\beta}{v_a}\frac{n_T}{2}\right). \tag{102}$$

The ratio of the total neutral pressure at the center of the discharge and at the wall is

$$\frac{p_{NT}(x=0)}{p_{NT}(x=a)} = \frac{N_0}{N_W} = 1 - D. \tag{103}$$

We turn now to the plasma dynamics. The plasma ions are assumed collisionless, so that the plasma dynamics is as described in section 4.2. As mentioned above, for simplicity, we use a cold fluid model for the ions, instead of the more accurate free-fall model [2, 15, 16, 72, 79]. The plasma flux at the wall, $\Gamma_{\max} = n_0 c/2$ (equation (40)), equals in size to $\Gamma_N(x=a)$, so that

$$\frac{n_0 c}{2} = N_W v_a \tanh\left(-\frac{\beta}{v_a}\frac{n_T}{2}\right), \tag{104}$$

which is a relation between the plasma and neutral parameters. We therefore write the equivalent relations

$$\frac{N_0}{N_W} = \sqrt{1 - \left(\frac{n_0 c}{2N_W v_a}\right)^2} \Longrightarrow D = 1 - \sqrt{1 - \left(\frac{n_0 c}{2N_W v_a}\right)^2}. \tag{105}$$

Equation (41), that relates the electron temperature T to the total number of neutrals per unit area N_T, enables us to write an expression for the neutral depletion that does not depend explicitly on the electron temperature. Using equations (101) and (41), we write

$$D = 1 - \frac{1}{\cosh\left(\frac{\pi-2}{2}\frac{c}{v_a}\frac{n_T}{N_T}\right)}. \tag{106}$$

If N_T and n_T are known (as well as v_a), then T is determined, and the neutral depletion is given by equation (101) (or equation (106)). Otherwise, one more relation is available between the plasma and neutral variables. This relation is derived now. We write the continuity equation as

$$\frac{\mathrm{d}\Gamma_n}{\mathrm{d}\xi} = \frac{\beta n_0 a}{v_a}\sqrt{\Gamma_n^2 + \left[\frac{2N_0 v_a}{n_0 c}\right]^2}\left(1 + \sqrt{1-\Gamma_n^2}\right), \tag{107}$$

where $\Gamma_n = 2\Gamma/n_0 c$ (see equation (40)). The solvability condition,

$$\int_0^1 \frac{\mathrm{d}\Gamma_n}{\sqrt{\Gamma_n^2 + 1/(2D - D^2)}\left(1 + \sqrt{1-\Gamma_n^2}\right)} = \frac{\beta n_0 a}{v_a}, \tag{108}$$

relates the neutral depletion D to the parameter $\beta n_0 a/v_a$; here we have used the relation $[2N_0 v_a/n_0 c]^2 = 1/(2D - D^2)$.

Figures 9 and 10, taken from [77], show the normalized plasma density and normalized neutral density when neutral depletion is small and large respectively. In the case of large neutral depletion $(n_0 c/2N_W v_a)^2 = 0.99$, so that $D = 0.9$. In both cases the density of the collisionless plasma at the wall is half the maximal density. When neutral depletion is significant (figure 10), the profile of the plasma density is flat near the discharge center, and the plasma density is approximately uniform in most of the discharge, dropping to $n_0/2$ only in the wall vicinity. Note also that when neutral depletion is significant, the neutrals pressure is maximal at the discharge center $P_{N,n} = p_N/p_N(0)$, even though their density is minimal there, following equation (92). The total pressure, which is minimal at the discharge center (equation (99)), is not shown in the figures.

8. Collisional unthermalized neutrals—neutral pumping

In this section, collisional plasma is again treated, but collisional neutral dynamics is assumed, which is different than the collisional neutral dynamics assumed in sections 5 and 6. We assume that the neutrals are collisional, so that they do collide with ions, contrary to the collisionless neutrals analyzed in the previous section. However, as in the previous section, and differently from in sections 5 and 6, the neutrals are assumed here to move ballistically before they collide with

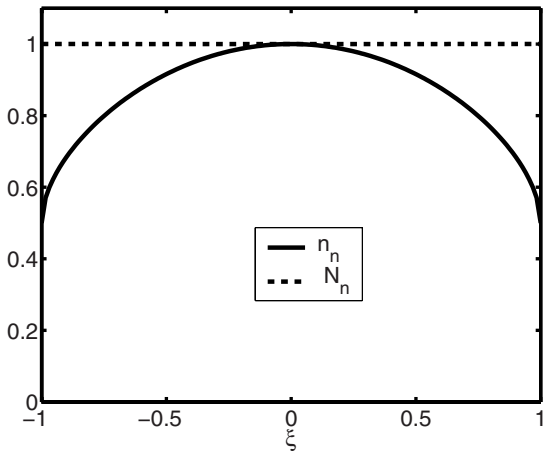

Figure 9. Neutrals are collisionless and unthermalized, planar geometry. Normalized plasma n_n and neutral N_n densities in the small depletion case. © 2008 IEEE. Reprinted, with permission, from [77].

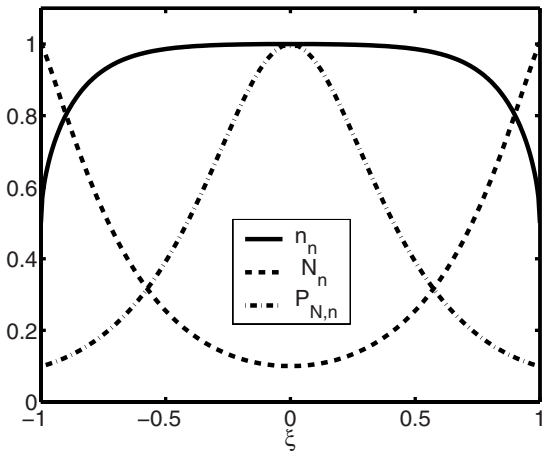

Figure 10. Neutrals are collisionless and unthermalized, planar geometry. Normalized plasma n_n and neutral N_n densities in the high depletion case, $D = 0.9$. The plasma density at the wall is half the maximal value. The neutrals pressure is highest where the neutral density is lowest, at the center. © 2008 IEEE. Reprinted, with permission, from [77].

an ion, without colliding between themselves, so that they are not thermalized. Such a situation can arise when the cross section for ion–neutral collision is larger than the cross section for neutral–neutral collision. The mean free path for ions between collisions with neutrals is then smaller than the mean free path for a neutral atom between its collisions with other neutrals. For example, according to the tables for argon on pages 568 and 570 in [141], for a large range of energies, the cross section for ion–neutral collision is more than ten times larger than the cross section for neutral–neutral collision. This means that if the length of the chamber is ten times larger than the mean free path for ion–neutral collision, an ion may collide ten times with neutrals, while a neutral experiencing a collision with an ion moves ballistically after such a collision, without colliding with another neutral before hitting the wall. The regime of validity for this picture is not large, but the picture allows a simple analysis, equivalent to the case of ion pumping in the previous section. When the neutral density is large, so that neutral–neutral collisions are more frequent, the simple analysis here ceases to be valid, and a model of thermalized neutrals, such as in the sections above, has to be used. An example of this intermediate density regime of neutrals, in which they experience collisions with ions but not between themselves, is also given for a flowing plasma later in the paper.

A neutral atom that encounters a collision with an ion acquires in the collision a high velocity towards the wall. This colliding neutral atom reaches the wall without any additional collision, either with an ion or with another neutral atom. The collisional neutral dynamics assumed here is therefore equivalent to the collisionless neutral dynamics assumed in the previous section; the collision event here replaces the ionization event of the collisionless case, both events removing neutrals from their slow ballistic motion, and causing them to move, fast, to the wall. Since neutrals are expelled through collisions, and not through ionization, the process belongs to what we call neutral pumping, which was analyzed in sections 5 and 6 (contrary to ion pumping).

The neutral dynamics assumed here is an approximation for a plasma in which $\beta \ll \beta_c$, and for a gas that is dilute enough so that neutral–neutral collisions are rare. The assumed neutral dynamics allows us a simple description of the plasma, and of neutral dynamics with neutral depletion. The analysis in this section follows the analysis in [78, 90].

The neutrals move ballistically either to the right (positive x) with a particle flux density $\Gamma_1(x)$ and density $N_1(x)$, or to the left with a particle flux density $\Gamma_2(x)$ and density $N_2(x)$. For simplicity, the neutral gas is taken as composed initially of two monoenergetic counter-streaming beams, as in the case of collisionless neutrals in the previous section. Therefore, all neutrals are assumed to have a velocity of the same magnitude $v_a = \Gamma_1(x)/N_1(x) = \Gamma_2(x)/N_2(x)$. Some of the neutrals gain a large velocity towards the wall through collisions with fast ions. This neutral pumping is the fast removal of the colliding neutrals from the discharge towards the wall. The fast component of the neutral flow is of a flux density $\Gamma_3(x)$ and density $N_3(x)$, and is in the direction of the plasma flow. Once a fast neutral hits the wall, it is assumed to be reflected with the low velocity v_a. Particle conservation is expressed as

$$\Gamma + \Gamma_1 - \Gamma_2 + \Gamma_3 = \Gamma_m, \tag{109}$$

where Γ_m is the total particle flux density and

$$N = N_1 + N_2 + N_3. \tag{110}$$

The continuity equations for the various species are

$$\frac{\mathrm{d}\Gamma}{\mathrm{d}x} = \beta\left(N_1 + N_2 + N_3\right)n, \quad \frac{\mathrm{d}\Gamma_1}{\mathrm{d}x} = -\beta N_1 n - \beta_c N_1 n,$$
$$\frac{\mathrm{d}\Gamma_2}{\mathrm{d}x} = \beta N_2 n + \beta_c N_2 n, \tag{111}$$

and

$$\frac{\mathrm{d}\Gamma_3}{\mathrm{d}x} = \beta_c\left(N_1 + N_2\right)n - \beta N_3 n. \tag{112}$$

Ion–neutral collisions may generate a wide distribution of neutral velocities, so that the distinction between a slow component and a fast component of the neutrals is not that

clear. Such collisions then lead to heating and thermalization of the neutral gas, as modeled in section 5. If the dominant collisions are charge exchange collisions, the colliding neutrals are expected to gain a high velocity directed along the ambipolar electric field towards the wall. This is the case that we model in this section, treating separately a slow component and a fast component of the neutrals. In recent years, configurations for plasma thrusters have been proposed, in which the thrust is provided by accelerated neutrals. Some configurations rely on neutral-gas heating [100, 102], while others rely on accelerating neutrals through charge exchange collisions without necessarily heating the gas [90, 116, 126].

We continue the analysis by treating separately the slow component and the fast component of the gas. We assume that the velocity of the fast neutrals is so high and their flux is not too large, so that the density of the fast neutrals is much lower than the density of the slow neutrals,

$$N_3 \ll N_1, N_2. \tag{113}$$

Because of their low density, the ionization of the fast neutrals is small. As said above, we also assume that neutrals do not collide and thermalize, so that the three neutral populations remain distinct. We therefore approximate the continuity equations as

$$\frac{\mathrm{d}\Gamma}{\mathrm{d}x} = \beta\left(N_1+N_2\right)n,\ \frac{\mathrm{d}\Gamma_1}{\mathrm{d}x} = -\beta_c N_1 n,$$
$$\frac{\mathrm{d}\Gamma_2}{\mathrm{d}x} = \beta_c N_2 n,\ \frac{\mathrm{d}\Gamma_3}{\mathrm{d}x} = \beta_c\left(N_1+N_2\right)n. \tag{114}$$

From these approximated equations, we derive the relation

$$\Gamma_3 = \frac{\beta_c}{\beta}\Gamma \gg \Gamma. \tag{115}$$

The relation (115) results in the flux of fast neutrals being larger than the plasma flux, leading (not necessarily but usually) to the force exerted by the neutrals, rather than the ion momentum, balancing the plasma pressure. The mass conservation is therefore approximated as

$$\Gamma_1 - \Gamma_2 + \frac{\beta_c}{\beta}\Gamma \cong \Gamma_m. \tag{116}$$

The slow neutrals are converted into fast neutrals and (at a smaller rate) into ions. We address in this section only cases of zero net flux, $\Gamma_m = 0$. The equations now are identical to those in the previous case of ion pumping, with the difference that the flux of the slow neutrals $\Gamma_N \equiv \Gamma_1 - \Gamma_2$ is balanced mostly by the flux of the fast neutrals, $\Gamma_3 = (\beta_c/\beta)\,\Gamma$, instead of by the flux of the ions, Γ. Equivalently to the previous section on ion pumping, we write for the variables of the slow neutrals,

$$\Gamma_N = \frac{N_W v_a}{\cosh\left(\frac{\beta_c}{v_a}\frac{n_T}{2}\right)}\sinh\left(-\frac{\beta_c}{v_a}\int_0^x n\left(x'\right)\mathrm{d}x'\right), \tag{117}$$

$$N = \frac{N_W}{\cosh\left(\frac{\beta_c}{v_a}\frac{n_T}{2}\right)}\cosh\left(-\frac{\beta_c}{v_a}\int_0^x n\left(x'\right)\mathrm{d}x'\right), \tag{118}$$

and

$$V = v_a\tanh\left(-\frac{\beta_c}{v_a}\int_0^x n\left(x'\right)\mathrm{d}x'\right). \tag{119}$$

The expressions for the slow neutral variables are identical to the expressions for the neutrals derived in the previous section for ion pumping, β_c replacing here β of the ion pumping case. From the expression for the neutral density, it follows that

$$N_0 = \frac{N_W}{\cosh\left(\frac{\beta_c}{v_a}\frac{n_T}{2}\right)}, \tag{120}$$

so that the neutral depletion is

$$D \equiv 1 - \frac{N_0}{N_W} = 1 - \frac{1}{\cosh\left(\frac{\beta_c}{v_a}\frac{n_T}{2}\right)}, \tag{121}$$

equivalently to the case of ion pumping.

We now relate the neutral flux at the wall to the plasma flux there,

$$\Gamma\left(x=a\right) = n_0 c\left(\frac{\beta}{\beta_c}\right)^{1/2} = \frac{\beta}{\beta_c}\Gamma_N = \frac{\beta}{\beta_c}N_W v_a\tanh\left(-\frac{\beta_c}{v_a}\frac{n_T}{2}\right). \tag{122}$$

Following equation (90), we express the neutral depletion in terms of the plasma maximal density n_0 and total number per unit area n_T,

$$\frac{N_0}{N_W} = \sqrt{1-\frac{\beta_c}{\beta}\left(\frac{n_0 c}{N_W v_a}\right)^2} \Longrightarrow D = 1 - \frac{1}{\cosh\left(\frac{\beta_c}{v_a}\frac{n_T}{2}\right)}$$
$$= 1 - \sqrt{1-\frac{\beta_c}{\beta}\left(\frac{n_0 c}{N_W v_a}\right)^2}. \tag{123}$$

With the relation between the electron temperature and the total number of neutrals per unit area, equation (37), we write the last expression as

$$\frac{N_0}{N_W} = \sqrt{1-\left(\frac{\beta_c n_0 N_T}{\pi N_W v_a}\right)^2} \Longrightarrow D = 1 - \sqrt{1-\left(\frac{\beta_c n_0 N_T}{\pi N_W v_a}\right)^2}. \tag{124}$$

The equation for Γ in equations (114) becomes

$$\frac{\mathrm{d}\Gamma_n}{\mathrm{d}\xi} = \frac{\beta_c n_0 a}{v_a}\sqrt{\Gamma_n^2\left(\xi\right) + \frac{N_0^2 v_a^2 \beta}{n_0^2 c^2 \beta_c}}\sqrt{1-\Gamma_n^2}. \tag{125}$$

The solvability condition is

$$\int_0^1 \frac{\mathrm{d}\Gamma_n}{\sqrt{1-\Gamma_n^2}\sqrt{\Gamma_n^2\left(\xi\right) + \left(1-D\right)^2/\left(2D-D^2\right)}} = \frac{\beta_c n_0 a}{v_a}, \tag{126}$$

which is written with the usual auxiliary variable $\theta = \arcsin\Gamma_n$ as

$$\int_0^{\pi/2} \frac{\mathrm{d}\theta}{\sqrt{\sin^2\theta + \left(1-D\right)^2/\left(2D-D^2\right)}} = \frac{\beta_c n_0 a}{v_a}. \tag{127}$$

The solvability condition relates $\beta_c n_0 a/v_a$ to the neutral depletion D, or, equivalently to $N_T/\pi N_W a$.

Figure 11, taken from [78], shows the normalized density profiles of the plasma and of the neutrals, for a high depletion case. Neutrals are collisional, and $(\beta_c/\beta)\left(n_0 c/N_W v_a\right)^2 = 0.9999$, resulting in $D = 0.99$. Such a configuration with ion–neutral collisions, as described in section 8, has been considered for a plasma thruster [90, 116].

9. Collisionless thermalized neutrals—neutral repletion

In all cases discussed so far, the interaction between the plasma and neutrals resulted in neutral depletion, the neutral-gas density being lower at the center of the discharge than near the discharge wall. Here, we examine the possibility suggested in [72, 79, 89]—termed 'repletion'—of the neutral-gas density being higher at the center of the discharge than near the wall. It is shown that it is not clear whether the conditions for the realization of repletion—frequent neutral–neutral collisions and rare neutral–ion collisions—can actually be satisfied.

In discussing equation (6), we have shown that the total neutral pressure, p_{NT}, increases monotonically towards the wall. In the purely collisionless case of ion pumping, it was shown in section 6 that despite that increase of the total neutral pressure towards the wall, p_N is maximal at the discharge center, and decreases towards the wall. The neutral density N, however, increases towards the wall. If neutrals still hardly collide with ions, but neutral–neutral collisions thermalize the neutrals so that their pressure is $p_N = NT_g$ and T_g is uniform, then, if the maximal p_N is at the discharge center, so is the maximal N. Neutral repletion is expected, in which p_N decreases towards the wall, while the total pressure increases towards the wall. We therefore examine equation (17)

$$\left(c_N^2 - V^2\right)\frac{\mathrm{d}N}{\mathrm{d}x} = \frac{S}{N}\Gamma_N - \beta_c N\Gamma_N, \tag{128}$$

where $c_N \equiv \sqrt{T_g/m}$ is the uniform gas sound speed. Note that the first term on the RHS, which is the contribution of ionization to the neutral momentum, does not increase with the neutral density. This is because, for a specified Γ_N, an increase of neutral density N results in a lower velocity V, and thus a lower momentum transfer.

Let us now examine the case that $S/N > \beta_c N$, so that the neutral density decreases towards the wall (note that $\Gamma_N < 0$ for $0 \leqslant x \leqslant a$). The case that the collisions term can be neglected, $S/N \gg \beta_c N$, can be solved analytically. In this case, equation (5) and equation (6) (in which the second term on the RHS is neglected) are combined to give

$$V^2 = \frac{\Gamma_N^2}{N^2} = c_N^2 \ln\left(\frac{N_0^2}{N^2}\right),\ p_{NT} = NT_g\left[1 + \ln\left(\frac{N_0}{N}\right)^2\right], \tag{129}$$

where $N_0 = N(x=0)$. Since $V \leqslant c_N$, the last relation yields bounds on the maximum variation of neutral density and pressure. These are

$$N_W \leqslant N_0 \leqslant 1.649 N_W, \quad p_{NT}(x=a) \geqslant p_{NT}(x=0) \geqslant 0.8245 p_{NT}(x=a), \tag{130}$$

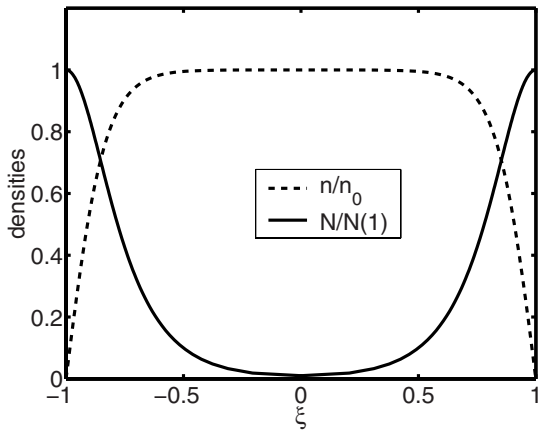

Figure 11. Neutrals are collisional and unthermalized, planar geometry. Normalized plasma and neutral densities in the high depletion case, $D = 0.99$. The plasma density at the wall is zero. Reproduced from [78].

where $\exp(1/2) = 1.649$.

It is seen in equation (130) that if the peak density is at the center, the variation of neutral density is not large. In the following analysis we can regard the neutral density as approximately constant, $N \cong N_W$. The source term can be estimated as $S \approx \Gamma/a$ and since $\Gamma = -\Gamma_N \leqslant N_W c_N$, we find that $S/N \leqslant c_N/a$. The requirement for the occurrence of repletion, $S/N > \beta_c N$, becomes $\beta_c N a/c_N \leqslant 1$. We can express the ion–neutral collision rate constant as $\beta_c \cong \sigma_{iN}(v - V)$ if $|v - V| > c_N$ or as $\beta_c \cong \sigma_{iN} c_N$ if $|v - V| < c_N$, where σ_{iN} is the ion–neutral collision cross section. In both cases, we can write the requirement for the occurrence of repletion as $\sigma_{iN} N a \leqslant 1$. The cross-section for neutral–neutral collisions σ_{NN} is expected to satisfy $\sigma_{NN} \leqslant \sigma_{iN}$, so that the requirement for repletion to occur results in

$$\frac{a}{\lambda_{NN}} < 1, \tag{131}$$

where $\lambda_{NN} \equiv 1/\sigma_{NN} N$ is the neutral–neutral collision mean free path. This means that neutral-neutral collisions should be rare. However, in the case that neutral–neutral collisions are rare, it is hard to assume that T_g is uniform, as we assumed in order for repletion to occur. Note that the analysis above did not rely on the plasma dynamics.

In summary, the analysis presented here suggests that there is no regime in which the drag by ions is small, and—simultaneously—neutral–neutral collisions are frequent. It could be, therefore, that neutral repletion does not occur, and only neutral depletion can occur.

10. Magnetized plasmas

We analyze here neutral depletion in a magnetized plasma. Magnetic field parallel to the wall and an ambipolar motion of the plasma across the magnetic field towards the wall are assumed. The neutrals move from the wall towards the discharge center. The motion either of the plasma or of the neutrals along the magnetic field is neglected, assuming that the system dimension along the magnetic field is much larger than across the magnetic field.

In analysing cross-field transport of a plasma, sometimes it is assumed that the flow is not ambipolar. Ions only cross magnetic field lines in the plasma, while electrons leave the plasma along the field lines and unite with ions at the plasma boundaries. The net charge crossing the plasma boundaries is zero, so that the flow is ambipolar globally, but is nonambipolar locally. This mechanism for nonambipolar flow is called the short circuit effect [112, 85, 94, 107]. In [85], we examined neutral depletion in magnetized plasmas for various cross-field transport mechanisms, in both ambipolar and nonambipolar plasma flows. In the analysis here, however, we restrict ourselves to ambipolar flow (the plasma flow is ambipolar also locally), as analyzed in [85] and also in [86].

Our interest here is the influence of the magnetic field on neutral depletion. The question we would like to answer is whether neutral depletion increases or decreases when the magnetic field is increased. It was pointed out in [86] that increasing the magnetic field while the plasma density is kept fixed seems to weaken neutral depletion. It was also pointed out that the simultaneous effect of that increase of magnetic field on other discharge parameters should be considered. We find that indeed it has to be specified how other control parameters vary when the magnetic field is varied. We examine the effect of varying the magnetic field when either the plasma density or the plasma particle flux density is kept constant. It is shown that if it is the plasma density that is kept constant while the magnetic field is varied, then neutral depletion indeed decreases with the magnetic field. However, if plasma particle flux is kept constant while the magnetic field is varied, then neutral depletion does not vary when the magnetic field is varied.

In the following discussion, we show through examining dimensionless parameters how the magnetic field affects neutral depletion while either plasma density, electron temperature, or plasma particle flux is kept constant; the reader may prefer to skip the detailed analysis and to read subsection 10.3, where numerical results are given.

The momentum equation for the plasma, equation (2), is first approximated as

$$\frac{\mathrm{d}\left(nT\right)}{\mathrm{d}x} = -m\beta_c N\Gamma - \frac{m_e\omega_c^2}{\nu_e}\Gamma. \tag{132}$$

The relative dominance of the two terms on the RHS of equation (132) reflects the relative dominance of neutrals pressure and magnetic pressure in balancing the plasma pressure. The associated competition between neutral depletion and diamagnetism has been studied recently experimentally [114] and theoretically [142]. The results of [114] are described briefly in subsection 10.3. We examine here the case that the magnetic field is strong enough, so that we neglect the drag on the ions due to collisions with neutrals. The momentum equation for the plasma is then

$$\frac{\mathrm{d}\left(nT\right)}{\mathrm{d}x} = -\frac{m_e\omega_c^2}{\nu_e}\Gamma. \tag{133}$$

In an ambipolar flow, the diffusion across magnetic field lines is determined by the electrons, because of their smaller cross-field mobility. Electrons cross field lines either due to collisions with neutrals or due to collisions with ions. We assume no anomalous cross-field transport. The collision frequency is therefore written as

$$\nu_e = \beta_{eN}N + \beta_{ei}n. \tag{134}$$

Here β_{eN} and β_{ei} are the electron–neutral and electron–ion collision rate constants, respectively (denoted in [85] as k_{eN} and k_{ei}). We turn to the neutral dynamics. The magnetic field does not affect the neutrals directly. As in sections 5 and 6, the pressure gradient of the neutrals is assumed to be balanced by the drag force exerted by the ions. We write equation (45) as

$$\frac{\mathrm{d}\left(NT_g\right)}{\mathrm{d}x} = m\beta_c N\Gamma. \tag{135}$$

Using equations (1) and (3), we write the continuity equation as

$$\frac{\mathrm{d}\Gamma}{\mathrm{d}x} = \beta Nn. \tag{136}$$

Equations (133)–(136) are the governing equations. The neutral depletion is found by solving these governing equations and finding N_0.

It is convenient to write the governing equations in a dimensionless form. These are

$$\frac{\mathrm{d}n_n}{\mathrm{d}\xi} = -\frac{\Gamma_B}{\left(b_{eN}N_n + b_{ei}n_n\right)}, \tag{137}$$

$$\frac{\mathrm{d}N_n}{\mathrm{d}\xi} = N_n\Gamma_B, \tag{138}$$

and

$$\frac{\mathrm{d}\Gamma_B}{\mathrm{d}\xi} = b_{\mathrm{ion}}N_n n_n, \tag{139}$$

where the dimensionless parameters are

$$b_{eN} \equiv \frac{Tm\beta_c\beta_{eN}N_W n_0}{T_g m_e\omega_c^2},\ b_{ei} \equiv \frac{Tm\beta_c\beta_{ei}n_0^2}{2T_g m_e\omega_c^2}, b_{\mathrm{ion}} \equiv \frac{m\beta_c\beta N_W n_0 a^2}{T_g}. \tag{140}$$

In [85], b_{eN} was denoted as $\overline{D_{\perp eN}}$ and b_{ei} was denoted as $\overline{D_{\perp ei}}/2$. The normalized variables are

$$n_n \equiv \frac{n}{n_0},\ N_n \equiv \frac{N}{N_W},\quad \Gamma_B \equiv \frac{m\beta_c a}{T_g}\Gamma. \tag{141}$$

Note that the dimensionless Γ_B in the magnetized plasma is different from the dimensionless Γ_n that we defined in section 4 for the unmagnetized plasma.

The boundary conditions for equations (137)–(139) are $n_n(0) = 1$ and $n_n(1) = 0$, while N_n and Γ_B are specified at one end only, $N_n(1) = 1$ and $\Gamma_B(0) = 0$. The solution of the equations, which expresses particle balance with these boundary conditions, thus provides one relation between the parameters, a relation that can be used to determine the value of one eigenvalue. In this set of nonlinear equations, however, both T and n_0 are unknown. We need another relation between the parameters. We may use power balance, equation (32), to further determine the discharge variables. For using equation (32), we need to know $\varepsilon_T(T)$ [10, 136], which is not easy to evaluate, considering the complex sheath of a magnetized plasma. In addition, as mentioned above, it is not clear whether the power

provided by the discharge generator is indeed the power deposited in the plasma that should be substituted in equation (32). In a helicon plasma source, the increase of power causes jumps in the plasma density, reflecting probably a sudden increase in the coupling of wave energy and plasma—a coupling that equation (32) is probably too simple to describe. We therefore prefer to examine how specifying the particle flux density at the wall, $\Gamma\,(x=a)$ ($\Gamma_{\max}$ in equation (32)), affects the discharge, instead of how specifying the power density P affects the discharge.

The equation for the neutral density can be replaced by an algebraic relation. We use equations (137) and (138) and the boundary condition $n_n(1)=0$ to derive a relation between the plasma density and neutral density [85],

$$N_n=\frac{\exp\left(-b_{ei}n_n^2\right)}{\left[1+b_{eN}\sqrt{\pi/\left(4b_{ei}\right)}\,\mathrm{erf}\left(\sqrt{b_{ei}}n_n\right)\right]}. \tag{142}$$

Here, erf denotes the error function. Neutral depletion is, therefore,

$$D\equiv 1-N_n(0)=1-\frac{\exp\left(-b_{ei}\right)}{\left[1+b_{eN}\sqrt{\pi/\left(4b_{ei}\right)}\,\mathrm{erf}\left(\sqrt{b_{ei}}\right)\right]}. \tag{143}$$

Neutral depletion depends on the two parameters, b_{eN} and b_{ei}, that depend on the plasma density n_0, the electron temperature T, and the magnetic field ω_c^2 (with the assumption that all other parameters are specified). To express neutral depletion as a function of ω_c^2 only, using equation (143), both n_0 and T have to be determined.

We note that relations (142) and (143) were derived by use of equations (137) and (138), which also hold in cylindrical geometry. Therefore, these relations between neutral density and plasma density, and the expression for the neutral depletion, are also valid for cylindrical geometry.

We mention again that the following detailed analysis in subsections 10.1 and 10.2 can be skipped, and the reader is referred to subsection 10.3.

As in [85], we treat two cases of ambipolar flow: one case that electrons collide mostly with neutrals, and the other case that electrons collide mostly with ions. We start with the case of dominant electron–neutral collisions.

10.1. Diffusion induced by electron collisions with neutrals

We assume that electron collisions with neutrals are more frequent than electron collisions with ions,

$$\beta_{eN}N\gg\beta_{ei}n, \tag{144}$$

and approximate $\nu_e=\beta_{eN}N$, so that cross-field diffusion of the electrons is induced by electron–neutral collisions. Equation (142) is simplified to

$$N_n=\frac{1}{1+b_{eN}n_n}, \tag{145}$$

while neutral depletion becomes

$$D=D_N=\frac{b_{eN}}{1+b_{eN}}. \tag{146}$$

The depletion D is larger for larger b_{eN}. From the dependence of the neutral depletion D on ω_c^2 (through b_{eN}); it follows that if the magnetic field is increased, while all other parameters are left unchanged, b_{eN} decreases; therefore, neutral depletion D decreases. These seemingly competitive effects of magnetic field and of neutral depletion when electron–neutral collisions are dominant were pointed out and analyzed in [86]. Experiments do not support this prediction. On the contrary, experiments seemed to show an increase of neutral depletion when the magnetic field was increased [75, 96]. As was also mentioned in [86], varying the magnetic field intensity, ω_c, is likely to cause n_0 to vary as well. In fact, in addition, the electron temperature, and, depending on the experimental conditions, also N_W may vary. Therefore, in order to understand the effect of the magnetic field on neutral depletion, we need to understand the effect of the magnetic field on all discharge parameters. We turn to include particle balance in the analysis, through the inclusion of the continuity equation, equation (1).

We combine equation (137), (139) and (145), to write the following nonlinear diffusion equation,

$$\frac{\mathrm{d}}{\mathrm{d}\xi}\left[\frac{1}{\left(1+b_{eN}n_n\right)}\frac{\mathrm{d}n_n}{\mathrm{d}\xi}\right]=-\alpha_{\perp eN}\frac{n_n}{1+b_{eN}n_n}, \tag{147}$$

where

$$\alpha_{\perp eN}\equiv\frac{b_{\mathrm{ion}}}{b_{eN}}=\frac{m_e\omega_c^2a^2\beta}{T\beta_{eN}}. \tag{148}$$

Solving equation (147), which expresses particle balance, with the boundary conditions $n_n(0)=1$ and $n_n(1)=0$, is solving an eigenvalue problem. If the value of $\alpha_{\perp eN}$ is specified, the value of b_{eN}, and also—as a result—the neutral depletion, are determined. We thus have to find the relation between these two parameters by solving the equation.

We note that for the low depletion case, $b_{eN}\ll 1$, we obtain for our assumed slab geometry the standard solution, $\cos\left[(\pi/2)\,\xi\right]$, and from the boundary conditions, we obtain the value of the eigenvalue,

$$\alpha_{\perp eN}=\frac{m_e\omega_c^2a^2\beta}{T\beta_{eN}}=\frac{\pi^2}{4}. \tag{149}$$

Equation (149) shows that in the low depletion limit, an increase of the magnetic field results in a lower β/T, and a lower electron temperature T.

We turn to a finite neutral depletion. Equation (147) can be integrated to

$$\frac{1}{\left(1+b_{eN}n_n\right)}\frac{\mathrm{d}n_n}{\mathrm{d}\xi}=-\frac{\sqrt{2\alpha_{\perp eN}}}{b_{eN}}\sqrt{\frac{1}{1+b_{eN}}-\frac{1}{1+b_{eN}n_n}+\ln\left(\frac{1+b_{eN}}{1+b_{eN}n_n}\right)}. \tag{150}$$

Integrating equation (150), and imposing the boundary conditions, $n_n(0)=1$ and $n_n(1)=0$, provide a relation between the two parameters b_{eN} and b_{ion} (or, equivalently, $\alpha_{\perp eN}$). Figure 12 is taken from [85]. The solid line in figure 12 shows $\sqrt{\alpha_{\perp eN}}$ as a function of $d\equiv N_W/N_0-1$, which we defined in [85] as the neutral depletion. The explicit relation between d and D, which we define as neutral depletion in this paper (equation (19)), is $D=d/(1+d)$. The relation between $\sqrt{\alpha_{\perp eN}}$ and D (through d) in figure 12 is informative. It shows that if $\sqrt{\alpha_{\perp eN}}$

is increased, so does the neutral depletion D (or d). Let us examine the effect of the magnetic field on the neutral depletion that follows this relation. We note that m_e, m, a, N_w, T_g, β_{eN} and β_c are assumed constant as ω_c^2 or T varies.

10.1.1. Effect of magnetic field on neutral depletion when plasma density is specified. Let us assume, first, that n_0 is specified and does not vary when ω_c^2 varies. It is clear that when ω_c^2 is increased, b_{eN} should decrease, because the variation of T is much smaller than that of ω_c^2. Neutral depletion thus decreases (with the decrease of b_{eN}). The accompanying decrease of $\sqrt{\alpha_{\perp eN}}$ according to figure 12 in this case must be due to a significant decrease of T, such that $\omega_c^2\beta/T$ decreases despite the increase of ω_c^2. In summary, if the plasma maximal density is specified, increasing the magnetic field results in a decrease of the electron temperature and a decrease of neutral depletion, as was shown in [86].

10.1.2. Effect of magnetic field on neutral depletion when electron temperature is specified. Let us assume now that the electron temperature is specified, and does not vary when ω_c^2 varies. In that case $\sqrt{\alpha_{\perp eN}}$ is linearly proportional to the magnetic field. An increase of the magnetic field results in an increase of b_{eN}, and consequently in an increase of the neutral depletion D_N. The plasma density n_0 increases at a faster rate than does ω_c^2.

So far we saw that an increase of the magnetic field while the plasma density is specified results in a decrease of electron temperature and neutral depletion, while an increase of the magnetic field while the electron temperature is specified results in an increase of both the plasma density and neutral depletion.

10.1.3. Effect of magnetic field on neutral depletion when plasma particle flux density at the wall is specified. Since $m\beta_c a/T_g$ is assumed constant as ω_c^2 or T varies, specifying Γ at the wall also specifies Γ_B at the wall, according to equation (141). In equations (137)–(139) at the limit (144), there are two parameters, b_{eN} and $b_{\rm ion}$. Specifying both n_n and Γ_B at both ends, $\xi = 0$ and $\xi = 1$, makes the two parameters eigenvalues that are determined by these two pairs of boundary conditions, and specifically by $\Gamma_B(1)$. With equation (137), the plasma particle flux density is expressed as

$$\Gamma_B = \sqrt{2\alpha_{\perp eN}}\sqrt{\frac{1}{1+b_{eN}} - \frac{1}{1+b_{eN}n_n} + \ln\left(\frac{1+b_{eN}}{1+b_{eN}n_n}\right)}. \tag{151}$$

The particle flux density at the wall $\Gamma_B(1)$ is

$$\Gamma_B(1) = \sqrt{2\alpha_{\perp eN}}\sqrt{\frac{1}{1+b_{eN}} - 1 + \ln(1+b_{eN})}. \tag{152}$$

Equation (152) provides a second relation between b_{eN} and $b_{\rm ion}$ (or, equivalently, $\alpha_{\perp eN}$). The first relation was obtained from the solution of equation (150) with the imposed boundary conditions. The two relations determine the values of the two parameters. Once b_{eN} is determined, so is the neutral depletion D_N. Neutral depletion is therefore determined once the plasma particle flux density is specified, and does not vary when the magnetic field varies. As b_{eN} and $b_{\rm ion}$ are constant for a constant $\Gamma_B(1)$, it follows that Tn_0/ω_c^2 and βn_0 are constant.

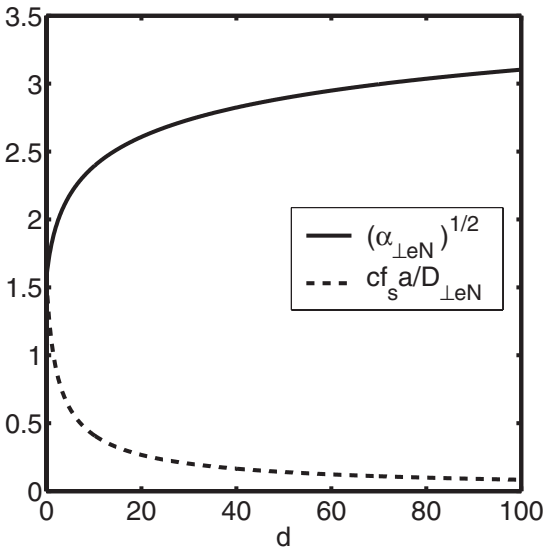

Figure 12. Magnetized plasma, planar geometry. Ambipolar cross-field diffusion induced by electron collisions with neutrals. Shown are $\sqrt{\alpha_{\perp eN}}$ (solid line) and $\Gamma_{\max}a/n_0D_{\perp eN}$ (dashed line) as a function of the neutrals depletion, $d = D/(1-D)$. The figure is taken from [85] and the legend for the dashed line is according to the notations there ($D_{\perp eN} = b_{eN}T_g/(n_0m\beta_c)$). At $D = 0$, $\sqrt{\alpha_{\perp eN}} = \Gamma_{\max}a/n_0D_{\perp eN} = \pi/2$. For $D \longrightarrow 1$, asymptotic expressions are presented in [85]. Reproduced from [85]. © IOP Publishing Ltd. All rights reserved.

It then follows that $\omega_c^2\beta/T$ is constant. An increase of ω_c^2 is followed by a decrease of β/T, i.e. a decrease of T which is followed by an increase of n_0. In summary, an increase of the magnetic field for a specified plasma particle flux density at the wall, is followed by an electron temperature decrease and a plasma density increase, while neutral depletion does not change.

We note that the dependence of neutral depletion demonstrated in this subsubsection is not surprising, as in equation (138) the neutral spatial derivative is proportional to the particle flux density.

10.2. Diffusion induced by electron collisions with ions

We now analyze the case that electron collisions with ions are more frequent than electron collisions with neutrals,

$$\beta_{ei}n \gg \beta_{eN}N. \tag{153}$$

We approximate $\nu_e = \beta_{ei}n$, so that cross-field diffusion of the electrons is induced by electron–ion collisions. We perform an analysis equivalent to the analysis in the previous section.

Equation (142) is reduced to the following relation between N and n,

$$N_n = \exp\left(-b_{ei}n_n^2\right). \tag{154}$$

The depletion is now expressed as

$$D = D_{ei} \equiv 1 - \exp\left(-b_{ei}\right). \tag{155}$$

The depletion D is larger for larger b_{ei}. From the dependence of the neutral depletion D on ω_c^2 (through b_{ei}), it is clear, as in the case of dominant electron–neutral collisions, that if the

magnetic field is increased, while all other parameters are left unchanged, b_{ei} decreases, i.e. neutral depletion D decreases. We continue the analysis as in the previous case (section 10.1), and we turn to include in the analysis particle balance through the inclusion of the continuity equation, equation (1).

Equivalently to the previous case, we derive the following nonlinear diffusion equation,

$$\frac{\mathrm{d}}{\mathrm{d}\xi}\left(n_n\frac{\mathrm{d}n_n}{\mathrm{d}\xi}\right) = -\alpha_{\perp ei}\exp\left(-b_{ei}n_n^2\right)n_n, \tag{156}$$

where

$$\alpha_{\perp ei} \equiv \frac{b_{\mathrm{ion}}}{b_{ei}} = \frac{m_e\omega_c^2a^2\beta N_W}{T\beta_{ei}n_0}. \tag{157}$$

Note that the nonlinearity on the LHS of equation (156) is a result of dominant electron–ion collisions, and not of neutral depletion. This nonlinear equation, when there is no neutral depletion (approximating $n_n^2 = 0$ in the argument of the exponent on the RHS of the equation), has been solved in [85]. Here, we solve the equation with neutral depletion. Before we do that we note that equation (156) is an eigenvalue problem, and its solution relates the two parameters, $\alpha_{\perp ei}$ and b_{ei}, and determines the neutral depletion D (through equation (155)), once $\alpha_{\perp ei}$ is specified, or additional relation between the two parameters is available.

Equation (156) is integrated to

$$n_n\frac{\mathrm{d}n_n}{\mathrm{d}\xi} = -\sqrt{2\alpha_{\perp ei}}\sqrt{\int_{n_n}^{1} dn_n' n_n'^2\exp\left(-b_{ei}n_n'^2\right)}. \tag{158}$$

Equivalently to the previous subsection, integrating equation (158) and imposing the boundary conditions, $n_n(0) = 1$ and $n_n(1) = 0$, provides a relation between the two parameters b_{ei} and b_{ion} (or, equivalently, $\alpha_{\perp ei}$). It is easy to see that if $\sqrt{\alpha_{\perp ei}}$ is increased, so do b_{ei} and the neutral depletion D. Let us examine also in this case the effect of the magnetic field on the neutral depletion that follows this relation. As before, note that m_e, m, a, N_w, T_g, β_{ei} and β_c are assumed constant as ω_c^2 or T varies.

10.2.1. Effect of magnetic field on neutral depletion when plasma density is specified. We assume again first that n_0 is specified and does not vary when ω_c^2 varies. It is seen that when ω_c^2 is increased, both b_{ei} and $\sqrt{\alpha_{\perp ei}}$ decrease. The parameter b_{ei} decreases because of the increase of ω_c^2, while $\sqrt{\alpha_{\perp ei}}$ decreases due to the decrease of T that results in a decrease of β and an increase of β_{ei} (which is proportional to $T^{-3/2}$). In summary, if the plasma maximal density is specified, increasing the magnetic field results in a decrease of the electron temperature and a decrease of neutral depletion, as was for dominant electron–neutral collisions.

10.2.2. Effect of magnetic field on neutral depletion when electron temperature is specified. Let us assume now that the electron temperature is specified and that it does not vary when ω_c^2 varies. The requirement that $\sqrt{\alpha_{\perp ei}}$ and b_{ei} increase together can be fulfilled if n_0 grows when ω_c grows. It is easy to verify that the dependence of n_0 on ω_c should obey $0.5 < \partial\ln n_0/\partial\ln\omega_c < 2$.

In summary, if the electron temperature is specified, increasing the magnetic field results in an increase of the plasma density and of neutral depletion.

10.2.3. Effect of magnetic field on neutral depletion when plasma particle flux density at the wall is specified. Equation (138) shows that $\Gamma_B(\xi)$ determines $N_W - N_0$, and for specified N_W it determines neutral depletion. It is now examined how neutral depletion is determined by $\Gamma_B(1)$. We use equations (137) and (158) and write an expression for the plasma particle flux density,

$$\Gamma_B = b_{ei}\sqrt{2\alpha_{\perp ei}}\sqrt{\int_{n_n}^{1} dn_n' n_n'^2\exp\left(-b_{ei}n_n'^2\right)} \tag{159}$$

The particle flux density at the wall $\Gamma_B(1)$ is then

$$\Gamma_B(1) = \sqrt{\frac{\alpha_{\perp ei}\sqrt{b_{ei}}}{2}}\left[\sqrt{\pi}\,\mathrm{erf}\left(\sqrt{b_{ei}}\right) - 2\sqrt{b_{ei}}\exp\left(-b_{ei}\right)\right]. \tag{160}$$

Equation (160) provides a second relation between b_{ei} and b_{ion} (or, equivalently, $\alpha_{\perp ei}$). The first relation was obtained from the solution of equation (158) with the imposed boundary conditions. The two relations determine the values of the two parameters. Once b_{ei} is determined, so is the neutral depletion D_e. Therefore, once the plasma particle flux density at the wall is specified, neutral depletion is determined, and it does not vary when the magnetic field varies. As b_{ei} and b_{ion} are constant for a constant $\Gamma_B(1)$, it follows that $T\beta_{ei}n_0^2/\omega_c^2$ and βn_0 are constant as well. As a result $\omega_c^2\beta^2/T\beta_{ei}$ is also constant. As this quantity is constant, an increase of ω_c^2 is followed by a decrease of $\beta^2/T\beta_{ei}$, i.e. a decrease of T. A decrease of T is followed by an increase of n_0, as βn_0 is constant.

In summary, as for the case in the previous subsubsection, an increase of the magnetic field for a specified constant plasma particle flux density is followed by an electron temperature decrease and a plasma density increase, while neutral depletion does not change.

10.3. Numerical examples

We have found that if either electron–neutral collisions or electron–ion collisions are dominant, for a specified plasma particle flux density at the wall, varying the magnetic field intensity should not vary neutral depletion. Here, we solve numerically the case that electrons collide with both neutrals and ions, for which we have not reached conclusions analytically.

Figures 13–17 demonstrate the effect of magnetic field on neutral depletion in an argon plasma. No particular regime is assumed, and the full equations, Equations (132), (134), and (135), as well as equations (1) and (3), are solved numerically. Moreover, the magnetic field is not assumed uniform, and the diamagnetic effect is included. Total pressure balance between plasma pressure, neutral pressure, and magnetic pressure is assumed,

$$\frac{B^2}{2\mu_0} + nT + NT_g = \frac{B_0^2}{2\mu_0} + N_WT_g. \tag{161}$$

The diamagnetic effect is small in these examples. Cases with a significant diamagnetic effect have been studied in [114, 142] for a cylindrical geometry. As throughout most of this paper, the geometry is taken here as planar, and in the examples here the distance between the wall and the central plane is $a = 0.1$ m. In figures 13–15, the maximal plasma density n_0 is specified, while in figures 16 and 17 the particle flux density at the wall $\Gamma(x = a)$ is specified.

In figures 13–15, the neutral pressure at the wall is 2.5 Pa and the gas temperature is uniform, $T_g = 300$ K, so that the neutral density at the wall is $N_W = 6 \times 10^{20}$ m^{-3}. In figure 13 neutral depletion is presented versus B for two values of maximal plasma density, $n_0 = 5 \times 10^{18}$ m^{-3} and $n_0 = 5 \times 10^{19}$ m^{-3}. For the lower plasma density, $n_0 = 5 \times 10^{18}$ m^{-3}, a steady-state also exists for an unmagnetized plasma, since for $B = 0$ the plasma pressure is smaller than the neutral pressure at the wall, $n_0 T < 2.5$ Pa. The neutral depletion $D = 1 - N_0/N_W$ is shown for this specified plasma density, $n_0 = 5 \times 10^{18}$ m^{-3}, versus the magnetic field intensity, $0 \leqslant B \leqslant 600$ G. Electron collisions with neutrals are comparable in frequency with electron collisions with ions, so that none of equations (146) or (155) is a good approximation for D. Nevertheless, as described above for each regime (dominant electron–neutral or dominant electron–ion collisions) separately, neutral depletion D decreases with B. For the higher plasma density, $n_0 = 5 \times 10^{19}$ m^{-3}, the minimal magnetic pressure that together with the neutral pressure can balance the plasma pressure is for $B \approx 150$ G. At such a high plasma density electron–ion collisions are dominant. The plasma dynamics is well described by equations (133) and (153), and neutral depletion is well approximated by equation (155), $D \cong D_e$. Neutral depletion decreases with B, as it did in the lower magnetic field.

The normalized plasma and neutral density profiles as functions of $\xi \equiv x/a$ are shown in figure 14 for the higher of the two plasma densities, $n_0 = 5 \times 10^{19}$ m^{-3}, for two magnetic field intensities, $B = 150$ G and $B = 600$ G. Neutral depletion is almost complete, $D \cong 1$, for $B = 150$ G and is smaller, $D \cong 0.4$ for $B = 600$ G, as is also seen in figure 13. When neutral depletion is larger, the plasma density is flatter than when neutral depletion is smaller.

We define a normalized plasma (and neutral) particle flux density at the wall,

$$\Gamma_n \equiv \frac{\Gamma(x = a)}{N_W \sqrt{T_g/m_i}}. \tag{162}$$

Note that Γ_n is defined differently here than in equation (27). In our example, $\Gamma(x = a) = 1.5 \times 10^{23}$ m^{-2} s^{-1} when $\Gamma_n = 1$. Figure 15 shows Γ_n as a function of the magnetic field intensity for the two densities. As the magnetic field is increased the plasma confinement is improved, and the flux density decreases. The maximal Γ_n for the higher density is 0.3 (not shown in the figure).

In figures 16 and 17, the particle flux density at the wall is specified. The plasma and neutral steady-state is calculated for $\Gamma_n = 0.0025$ and for $\Gamma_n = 0.02$. Figure 16 shows the neutral depletion D, the maximal plasma density n_0 (in units of 10^{19} m^{-3}), and the electron temperature, denoted as Te (in eV), as functions of the magnetic field B. Variables

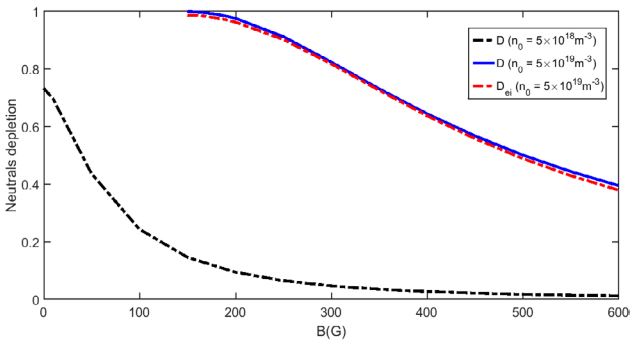

Figure 13. Magnetized plasma, planar geometry. Neutrals depletion $D = 1 - N_0/N_W$ as a function of the magnetic field intensity B, for $n_0 = 5 \times 10^{18}$ m^{-3} and for $n_0 = 5 \times 10^{19}$ m^{-3}. An argon plasma of neutrals pressure at the wall of 2.5 Pa and $T_g = 300$ K ($N_W = 6 \times 10^{20}$ m^{-3}), $a = 0.1$ m. For the higher density shown also D_{ei} (equation (155)), which is a good approximation for D.

that correspond to $\Gamma_n = 0.0025$ are denoted by the subscript 1, while those that correspond to $\Gamma_n = 0.02$ are denoted by the subscript 2. It is seen in the figure that the neutral depletion almost does not vary when the magnetic field varies, as we showed above separately for each collisional regime. For $\Gamma_n = 0.0025$ the neutral depletion is about $D = 0.20$, while for $\Gamma_n = 0.020$, it is about $D = 0.77$. In figure 17, the profiles of the dimensionless plasma and neutral densities are shown for the two plasma particle flux densities. The plasma density is flatter for $\Gamma_n = 0.02$, when neutral depletion is larger. The density profiles do not vary when the magnetic field varies, as long as the plasma particle flux density Γ_n does not vary. This result is not shown in the figures.

As mentioned above, neutral depletion in magnetized plasma was measured in [75, 96], and it seemed to increase when the magnetic field was increased. Magee *et al* [96] repeated their experiment when there was no flowing gas or flowing plasma in the (helicon) source. Neutral depletion did not increase, in that case, when the magnetic field was increased. It could be that the conditions in the experiment in [96] with no flow had similarity to the case analyzed here, where the magnetic field was increased but the plasma particle flux density at the wall did not change. In the experiment with a flowing plasma in [96], and probably also in the experiment in [75], experiments that showed an increase of neutral depletion when magnetic field was increased, the plasma particle flux density could have increased with the increasing magnetic field, which could have led to that increased neutral depletion. It could also be that plasma motion along the magnetic field, neglected in the analysis here, played a role in the experiments in [75, 96].

10.4. Suppressed diamagnetism

Recent measurements by Shinohara *et al* showed that the diamagnetic effect in a magnetized plasma was smaller than expected [114]. It was realized that the plasma pressure in a magnetized partially-ionized plasma is balanced by both magnetic field pressure and neutral pressure. Neutral pressure is expressed by the first term on the RHS of equation (132),

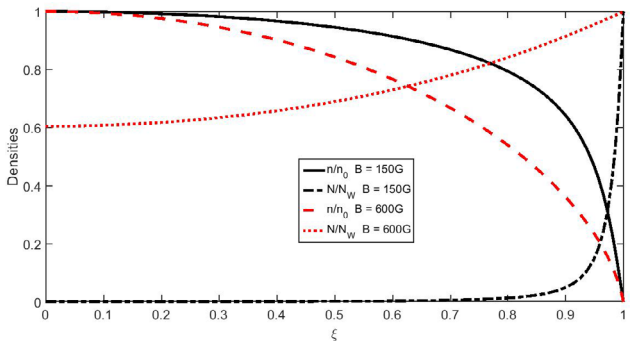

Figure 14. Magnetized plasma. The normalized plasma and neutrals density profiles as functions of $\xi \equiv x/a$ for $B = 150$ G and $B = 600$ G; $n_0 = 5 \times 10^{19}$ m^{-3}. As in figure 13, an argon plasma, neutrals pressure at the wall of 2.5 Pa and $T_g = 300$ K ($N_W = 6 \times 10^{20}$ m^{-3}), $a = 0.1$ m. Neutrals depletion is almost complete for $B = 150$ G and is smaller for $B = 600$ G. When neutrals depletion is larger, the plasma density is flatter near the discharge center than when neutrals depletion is smaller.

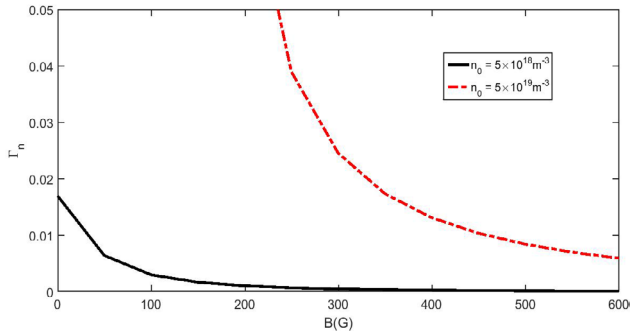

Figure 15. Magnetized plasma, planar geometry. The normalized plasma particle flux density at the wall Γ_n versus the magnetic field intensity B for $n_0 = 5 \times 10^{18}$ m^{-3} and for $n_0 = 5 \times 10^{19}$ m^{-3}. An argon plasma, pressure at the wall 2.5 Pa and $T_g = 300$ K ($N_W = 6 \times 10^{20}$ m^{-3}), $a = 0.1$ m. The maximal Γ_n for the higher density is 0.3 (not shown).

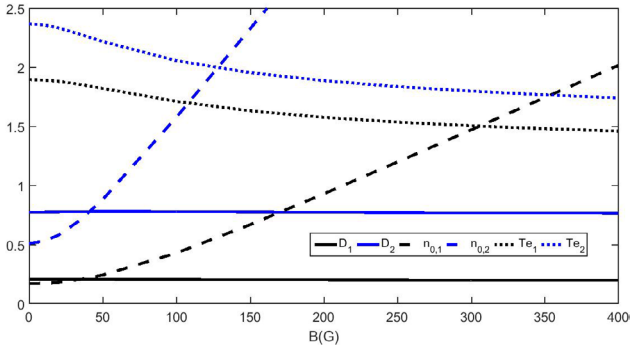

Figure 16. Magnetized plasma, planar geometry. Neutrals depletion D, the maximal plasma density n_0 (in units of 10^{19} m^{-3}), and the electron temperature Te (in eV) versus the magnetic field B, for $\Gamma_n = 0.0025$ (subscript 1) and for $\Gamma_n = 0.02$ (subscript 2). An argon plasma, the pressure at the wall 2.5 Pa and $T_g = 300$ K ($N_W = 6 \times 10^{20}$ m^{-3}), $a = 0.1$ m. $D_1 \cong 0.20$, $D_2 \cong 0.77$.

while the magnetic pressure is expressed by the second term on the RHS. It was shown in [114] that if

$$C \equiv \frac{e^2 B^2}{m m_e \nu_e \nu_i} < 1, \qquad (163)$$

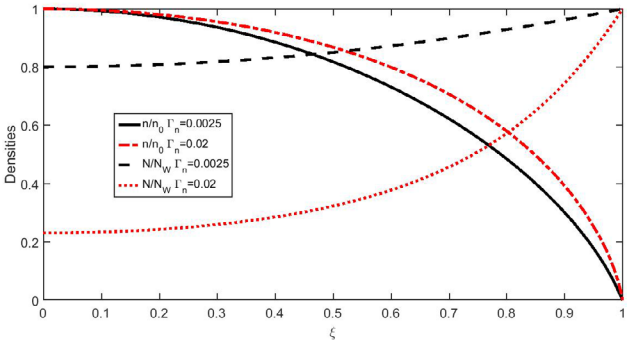

Figure 17. Magnetized plasma, planar geometry. The normalized plasma and neutrals density profiles as functions of $\xi \equiv x/a$ for $\Gamma_n = 0.0025$ ($n_0 = 2 \times 10^{19}$ m^{-3}) and for $\Gamma_n = 0.02$ ($n_0 = 6.1 \times 10^{19}$ m^{-3}). The plasma density profile is flatter near the discharge center for $\Gamma_n = 0.02$, when neutrals depletion is larger. An argon plasma, the pressure at the wall 2.5 Pa and $T_g = 300$ K ($N_W = 6 \times 10^{20}$ m^{-3}), $a = 0.1$ m. The density profiles do not vary when the magnetic field varies, as long as the particle flux density Γ_n does not vary. Here, $B = 400$ G.

diamagnetism is expected to be suppressed by neutral depletion. In that case, most of the plasma pressure is balanced by neutral pressure, and not by the magnetic pressure. Here, $\nu_i \equiv \beta_c N$ is the frequency of ion–neutral collisions. Note that C is not necessarily uniform across the discharge.

Figure 18, taken from [114], shows the measured decrease of magnetic field (the diamagnetism) as a function of B. It is shown that for a low B, the diamagnetic effect is lower than expected by the plasma beta. The parameter C at this regime is smaller than unity. Indeed, a solution of the model equations of this section in a cylindrical geometry that calculates the profile of B is in reasonable agreement with the measurement, and explains the suppressed diamagnetism. A detailed theoretical analysis is given in [142].

11. Flowing plasma

In many systems of interest there is a net mass flow. Neutrals are injected at one end of the discharge chamber, and a mixture of neutral and ionized gases flows out of the discharge chamber at the other end. Such configurations are used for industrial applications and for plasma thrusters. Helicon sources considered for propulsion [115–133] are one example of such a system with a net mass flow. When the helicon magnetic field is large, so that wall losses are small, a 1D model as in this paper can describe the flow dynamics approximately. This description is useful for the helicon plasma source itself, while where the magnetic field diverges beyond the source exit, a different model has to be used. The 1D analysis of the flowing plasma here follows [77] for a collisionless flow, with some results from [90] included for a collisional flow.

In the case of a net mass flow, the flow is not symmetrical with respect to the plane at the center of the discharge (for a slab geometry). The end of the channel at which the gas enters is denoted as $x = 0$, and the end at which the plasma–neutral flow exits is denoted as $x = L = 2a$. The neutral density decreases along the channel,

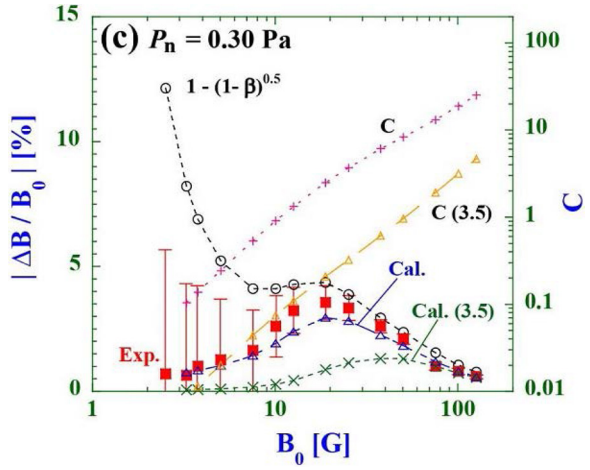

Figure 18. Measurements of the diamagnetic effect in a helicon source. The measured $\Delta B/B$ is much smaller than expected by the plasma beta but agrees with a model (of cylindrical geometry) that includes neutrals depletion. Reprinted from [114], with the permission of AIP Publishing.

$$\frac{\mathrm{d}N}{\mathrm{d}x} < 0. \tag{164}$$

It is assumed that the gas is introduced through holes in a wall that is located at $x = 0$. Therefore, neutrals move only in the positive x direction, away from the back wall. Ions and electrons that impinge on the back wall recombine, and the neutrals produced join the neutral flow in the positive x direction, as in the case of a non-flowing plasma. Ions are assumed collisionless, so that equation (31) becomes

$$\left(1 - M^2\right) \frac{\mathrm{d}M}{\mathrm{d}x} = \frac{\beta N}{c} \left(1 + M^2\right). \tag{165}$$

As we did before, we can relate the (assumed uniform) electron temperature to the total number of neutrals per unit area. Despite the asymmetry of the flow, ions are still assumed to reach the acoustic velocity at the two chamber ends. We first relate the number of neutrals to the ion Mach velocity. Equation (165) is integrated to

$$\frac{c}{\beta}\left(2\arctan M - M + \frac{\pi}{2}\right) = \int_0^x N\mathrm{d}x. \tag{166}$$

Integrating across the discharge chamber, we find the relation between the total number of neutrals per unit area and the electron temperature,

$$1.1416\frac{c}{\beta} = N_T = \int_0^L N\mathrm{d}x, \tag{167}$$

which is identical to equation (30) in the collisionless limit.

It is easily seen how neutral depletion in the flowing plasma causes the maximum of the plasma density to move towards the gas inlet end, at $x = 0$. The integral in equation (166) is split into two integrals:

$$0.5708\frac{c}{\beta} = \frac{c}{\beta}\int_{-1}^{0} \frac{\left(1 - M^2\right)}{\left(1 + M^2\right)}\mathrm{d}M = \int_0^{x_0} N\mathrm{d}x = \int_{x_0}^{L} N\mathrm{d}x. \tag{168}$$

Since the neutral density decreases away from $x = 0$, the neutral density in the integral of the third term in equation (168) is larger than the neutral density in the integral of the fourth term. The two integrals can be equal only if the interval of integration of the third term is shorter than the interval of integration of the fourth term. The result is that the location of the maximal density x_0, where $M = 0$, satisfies

$$x_0 < a. \tag{169}$$

Thus, due to neutral depletion, the location of the maximal plasma density shifts from the center of the discharge towards the gas inlet. As neutral depletion increases, so that the neutral density decreases everywhere away from the gas inlet, the location of the maximal plasma density, x_0, gets closer to the gas inlet end at $x = 0$.

Let us now specify the neutral dynamics. As in section 7, we assume that the neutral are monoenergetic. However, instead of the two monoenergetic beams flowing in opposite directions of the bounded plasma analyzed there, here, the neutrals constitute one monoenergetic beam only, flowing towards the exit. The neutral–gas distribution function at the gas-inlet is of the form

$$f_N(v) = N_0\delta\left(v - v_a\right), \tag{170}$$

where N_0 is the neutral density at the gas-inlet upstream. We write the net mass flow rate as

$$\Gamma + Nv_a = \Gamma_m \equiv \frac{\dot{m}}{S_r m}, \tag{171}$$

where Γ_m, the particle (neutral plus plasma) flux-density, is expressed as the ratio of $\dot{m}$, the mass flow rate, and the product of m and S_r, the channel cross-section. Since we assume that v_a is uniform in the channel, equation (171) determines the value of the varying neutral density N along the channel as a function of the varying ion flux density Γ. The neutral density is therefore:

$$N = \frac{1}{v_a}\left(\Gamma_m - \Gamma\right). \tag{172}$$

At the collisionless limit, equation (24) becomes

$$\Gamma = \frac{n_0 cM}{\left(1 + M^2\right)}. \tag{173}$$

These two last relations and equation (165) become

$$\left(1 - M^2\right)\frac{\mathrm{d}M}{\mathrm{d}x} = \frac{1}{\lambda_{\mathrm{ion}}}\left(M^2 + 1 - 2\eta_m M\right), \tag{174}$$

where

$$\eta_m \equiv \frac{\Gamma\left(x = L\right)}{\Gamma_m};\ \lambda_{\mathrm{ion}} \equiv \frac{v_a c}{\beta\Gamma_m}. \tag{175}$$

The ratio η_m is the propellant utilization and $\Gamma\left(x = L\right) = \Gamma_{\max} = n_0 c/2$ is the ion flux density at the gas exit from the source. Also, λ_{ion} is a characteristic ionization mean free path of the plasma flow.

The last equation can be integrated to

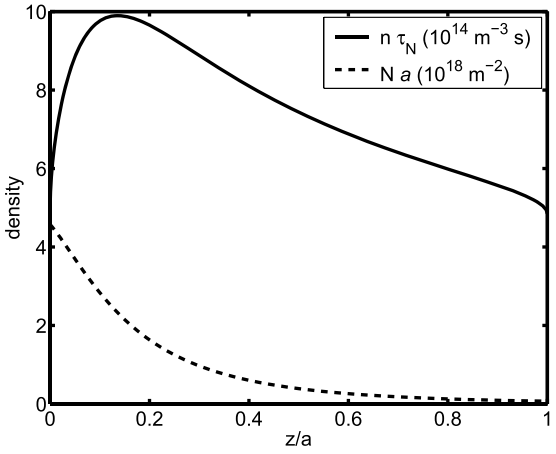

Figure 19. Flowing plasma. The profiles of the normalized plasma and neutral-gas densities in argon. The collisionality is low, $\beta_c/\beta = 0.1351$, and $T = 7$ eV. The propellant utilization is $\eta_m = 0.8553$ and the profile of the plasma density is asymmetrical, due to neutrals depletion by ionization. The gas inlet is on the left and the exit, which is the open boundary, is on the right. © 2011 IEEE. Reprinted, with permission, from [90]. z/a denotes x/L in this paper. For the legend see [90].

$$-1-M-\eta_m \ln\left(\frac{M^2+1-2\eta_m M}{2+2\eta_m}\right) + 2\sqrt{1-\eta_m^2}\left[\arctan\left(\frac{M-\eta_m}{\sqrt{1-\eta_m^2}}\right) - \arctan\left(\frac{-1-\eta_m}{\sqrt{1-\eta_m^2}}\right)\right] = \frac{x}{\lambda_{\text{ion}}}, \tag{176}$$

which satisfies $M = -1$ at $x = 0$. Requiring that $M = 1$ at $x = L$, we obtain

$$-2-\eta_m \ln\left(\frac{1-\eta_m}{1+\eta_m}\right) + 2\sqrt{1-\eta_m^2}\left[\arctan\left(\frac{1-\eta_m}{\sqrt{1-\eta_m^2}}\right) - \arctan\left(\frac{-1-\eta_m}{\sqrt{1-\eta_m^2}}\right)\right] = \frac{L}{\lambda_{\text{ion}}}. \tag{177}$$

The propellant utilization is determined by L/λ_{ion}, the number of ionization mean free paths along the channel. We can now write the profile of the ion flow velocity as

$$\frac{-1-M-\eta_m \ln\left(\frac{M^2+1-2\eta_m M}{2+2\eta_m}\right) + 2\sqrt{1-\eta_m^2}\left[\arctan\left(\frac{M-\eta_m}{\sqrt{1-\eta_m^2}}\right) - \arctan\left(\frac{-1-\eta_m}{\sqrt{1-\eta_m^2}}\right)\right]}{-2-\eta_m \ln\left(\frac{1-\eta_m}{1+\eta_m}\right) + 2\sqrt{1-\eta_m^2}\left[\arctan\left(\frac{1-\eta_m}{\sqrt{1-\eta_m^2}}\right) - \arctan\left(\frac{-1-\eta_m}{\sqrt{1-\eta_m^2}}\right)\right]} = \frac{x}{L}. \tag{178}$$

We define the rate of neutral depletion in this case of a net mass flow as

$$D \equiv 1 - \frac{N(x=L)}{N(x=0)}. \tag{179}$$

Since $N(x=0)\,v_a = \dot{m}/S_r m - \Gamma(0)$, $N(x=L)\,v_a = \dot{m}/S_r m - \Gamma(L)$ and $\Gamma(0) = -\Gamma(L)$ we obtain

$$D = \frac{2\eta_m}{1+\eta_m}. \tag{180}$$

At the limit of low ionization, equation (177) yields

$$\pi - 2 = \frac{L}{\lambda_{\text{ion}}} = \frac{\beta N L}{c},\ \eta_m \ll 1. \tag{181}$$

Here N is the constant neutral density.

At the opposite limit of large neutral depletion,

$$\eta_m = 1 - 2\exp\left[-\left(2+\frac{L}{\lambda_{\text{ion}}}\right)\right], \tag{182}$$

which is a slightly modified form of equation (66) in [77]. At that limit, the neutral depletion is

$$D = 1 - \exp\left[-\left(2+\frac{L}{\lambda_{\text{ion}}}\right)\right]. \tag{183}$$

The collisionless case detailed here was described in [77]. The analysis was generalized for a plasma flow with ion–neutral collisions in [90]. The collisions were treated not as raising the neutral temperature, rather at the limit of neutral pumping, similarly to that described in section 8. The argon-plasma flow described in figure 19 (taken from [90]), is of a relatively high electron temperature, $T = 7$ eV. For this T, β is large and $\beta_c/\beta = 0.1351$. In such a low ion–neutral collisionality plasma, the profiles obtained by calculations with ion-neutral collisions are described approximately by the analytical expressions given above when collisions are neglected. In this numerical example L/λ_{ion} is large, so that the propellant utilization is close to unity, $\eta_m = 0.8553$. Neutral depletion is high, $D = 0.922$, and, as a result, the asymmetry of the plasma density profile is large. Since the plasma is approximately collisionless, the plasma density at the two ends of the discharge is about half the maximal density.

While ion pumping, as described in section 7, dominates the flow analyzed above and demonstrated in figure 19, neutral pumping, as described in section 8, dominates the flow demonstrated in figure 20. In figure 20, $T = 1.9$ eV and $\beta_c/\beta = 129$ in an argon plasma. The propellant utilization is low, $\eta_m = 0.0073$. However, due to collisions, the neutral flow is also composed of energetic neutrals, and an equivalent propellant utilization is defined, η_{mc}, that expresses the fraction of pushed neutrals, which is large in figure 20, $\eta_{mc} = 0.95$. The plasma density profile is asymmetrical when neutrals are depleted through collisions, due to neutral pumping, equivalently to ion pumping as shown in figure 20. The analysis is detailed in [90].

The asymmetry of the profile of the plasma density has been demonstrated experimentally [83, 109, 111, 128]. The evolution in time of the plasma density, the profile changing from symmetrical to asymmetrical profile due to neutral depletion, has been recently demonstrated experimentally [111].

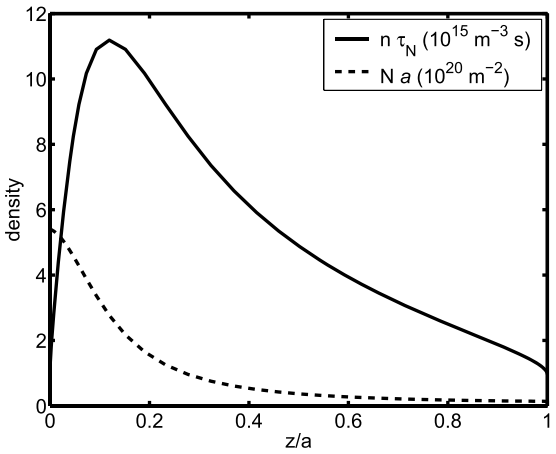

Figure 20. Flowing plasma. The profiles of the normalized plasma and neutral-gas densities in argon. The collisionality is high, $\beta_c/\beta = 129$, and $T = 1.9$ eV. The propellant utilization due to ionization is $\eta_m = 0.0073$, but that due to collisions is $\eta_{mc} = 0.95$. The profile of the plasma density is also asymmetrical, here due to neutrals depletion by ion–neutrals collisions. The gas inlet is on the left and the exit, which is the open boundary, is on the right. © 2011 IEEE. Reprinted, with permission, from [90]. z/a denotes x/L in this paper. For the legend see [90].

12. Summary

In this paper, we have reviewed the coupled plasma-neutral dynamics in a partially-ionized plasma. The neutral density profile modified by the interaction with the plasma and the change of the plasma density due to the modified neutral density were studied for various different neutral dynamics. The nonlinear interaction led to neutral depletion, a reduced neutral density at the center of the discharge chamber, where the plasma density is maximal.

We mention here the main results described in this paper. In a collisional plasma, neutral depletion is due to plasma pressure, a process we called neutral pumping. In such collisional plasma, when the plasma particle flux density is large (due to large ionization), an increase of the deposited power results in an unexpected decrease of the plasma density, despite the increase of the flux of generated plasma. The mechanism that causes the density decrease was shown to be the enhanced plasma transport due to neutral depletion. The nonmonotonic dependence was shown using semi-analytic expressions for a planar geometry, and numerically for cylindrical geometry.

Neutral depletion due to neutral-gas heating was then analysed. It was shown that gas heating can enhance neutral depletion dramatically. The gas heating was assumed to be due to electron–neutral collisions, and to be balanced by heat conduction to the wall. For a low ionization, the gas temperature increases with the plasma flux, and causes significant neutral depletion, even though the plasma pressure is still much smaller than the neutral-gas pressure. As ionization increases, the neutral-gas temperature starts to decrease. Thus, the gas temperature was shown to also vary nonmonotonically with the plasma particle flux density.

Neutral depletion due to ionization in a collisionless plasma—ion pumping—was described by a simple formalism. A similar formalism was adopted to describe neutral pumping in a plasma in which the number of collisions is small, a situation that could be explored for plasma thrusters. It was determined that it is not likely that the necessary conditions for the occurrence of neutral repletion can be satisfied. Therefore it looks as though neutral repletion cannot occur.

The effect of the magnetic field on neutral depletion in plasma in which cross-field diffusion is dominant was examined. It was found that neutral depletion does not vary with the magnetic field as long as the plasma particle flux is kept constant, while neutral depletion does decrease with the magnetic field, if it is the plasma density that is kept constant. Cases were identified in which neutral depletion suppresses plasma diamagnetism.

Flowing plasma in a configuration of a plasma thruster was studied. Conditions for high ionization (or large neutral depletion) were determined through an analytical solution that could be useful also for plasma thrusters. The analysis should be extended to address other devices such as negative ion sources [91–93, 103, 104].

In order to demonstrate the various forms of neutral depletion, we chose the simplest geometry that often allowed us to derive analytical results. In experiments the geometry is naturally more complex, 1D and time independent models are often not sufficient. By illuminating the basic processes, we hope that the models presented here could guide more complex numerical calculations.

Acknowledgments

The author had very helpful discussions with A Aanesland, U Czarnetzki, L Liard, R Magee, G Makrinich, J-L Raimbault, J-M Rax and H-B Valentini. This research was partially supported by the Israel Science Foundation (Grant no. 765/11).

References

[1] Schottky W 1924 *Phys. Z.* **25** 635
[2] Tonks L and Langmuir I 1929 A general theory of the plasma of an arc *Phys. Rev.* **34** 876
[3] Bohm D 1949 *The Characteristics of Electrical Discharges in Magnetic Fields* ed A Guthry and R K Wakerling (New York: MacGraw-Hill) ch 3 p 77
[4] Persson K B 1962 Inertia-controlled ambipolar diffusion *Phys. Fluids* **5** 1625
[5] Mosburg E R Jr and Persson K-B 1964 Nonlinear ambipolar diffusion of an isothermal plasma across a magnetic field *Phys. Fluids* **7** 1929
[6] Forrest J R and Franklin R N 1966 The positive column in a magnetic field at low pressures: the transition from free-fall to ambipolar conditions *Br. J. Appl. Phys.* **17** 1569
[7] Self S A and Ewald H N 1966 Static theory of a discharge column at intermediate pressures *Phys. Fluids* **9** 2486
[8] Franklin R N 1976 *Plasma Phenomena in Gas Discharges* (Oxford: Clarendon)
[9] Godyak V A 1986 *Soviet Radio Frequency Discharge Research* (Falls Church, VI: Delphic Associates)
[10] Lieberman M A and Lichtenberg A J 2005 *Principles of Plasma Discharges and Materials Processing* (New York: Wiley)

[11] Fruchtman A, Makrinich G and Ashkenazy J 2005 Two-dimensional equilibrium of a low temperature magnetized plasma *Plasma Sources Sci. Technol.* **14** 152

[12] Sternberg N, Godyak V and Hoffman D 2006 Magnetic field effects on gas discharge plasmas *Phys. Plasmas* **13** 063511

[13] Steenbeck M 1939 Theoretische und experimentelle untersuchungen tiber den einfluß des elektronenpartialdrucks in niederdrucksaulen *Wiss. Veroff. Siemens Werke* **18** 318 (in German)

[14] Allen J E and Thonemann P C 1954 Current limitation in the low pressure mercury arc *Proc. Phys. Soc.* B. **67** 768

[15] Caruso A and Cavaliere A 1964 The low pressure discharge in the strong ionization regime *Br. J. Appl. Phys.* **15** 1021

[16] Valentini H-B 1971 Geschwindigkeitsverteilung, teilchendichte, transversale driftgeschwindigkeit und energiedichte des neutralgases in der freifallsäule unter berücksichtigung der durch die ionisationsvorgänge *Beitr. Plasmaphysik* **11** 483 (in German)

[17] Torven S 1971 The neutral atom distribution function in a low pressure positive column *Phys. Scr.* **4** 65

[18] Stangeby P C and Allen J E 1971 Current limitation in mercury vapour discharges—I. Theory *J. Phys. A: Gen. Phys.* **4** 108

[19] Stangeby P C and Allen J E 1973 Current limitation in mercury vapour discharges—II. Experiment *J. Phys. D: Appl. Phys.* **6** 224

[20] Zendin L D 1973 *J. Techn. Phys.* **43** 1595

[21] Valentini H-B 1974 Das neutralgasprofil und die elektronentemperatur in der freifallsäule bei hohem ionisationsgrad *Beitr. Plasmaphysik* **14** 201 (in German)

[22] Valentini H-B 1976 Momentengleichungen für plasmen mit anisotropem neutralgasdruck und anisotropem ionendruck *Beitr. Plasmaphysik* **16** 181 (in German)

[23] Valentini H-B 1979 Theory of low pressure discharge *Beitr. Plasmaphysik* **19** 81

[24] Valentini H-B 1979 The theory of the low-pressure, high-current discharge column: the influence of the degree of ionization and of the neutral gas temperature on the radial profiles of the charged particle density, the neutral gas density and on the electron temperature *Beitr. Plasmaphysik* **19** 151

[25] Valentini H B 1984 Theoretical description of gas discharges containing excited atoms at low pressures *J. Phys. D: Appl. Phys.* **17** 931

[26] Shapiro D A and Valentini H-B 1991 Hydrodynamic theory of low pressure multi-component discharges with neutral gas depletion *Contr. Plasma Phys.* **31** 391

[27] Boswell R, Porteous R, Prytz A, Bouchoule A and Ranson P 1982 Some features of rf excited fully ionized low pressure argon plasma *Phys. Lett.* **91A** 163

[28] Boswell R W 1984 Very efficient plasma generation by whistler waves near the lower hybrid frequency *Plasma Phys. Control. Fusion* **26** 1147
Boswell R W and Porteous K 1987 Large volume, high density rf inductively coupled plasma *Appl. Phys. Lett.* **50** 1130

[29] Porteous R K and Boswell R W 1992 *Proc. of the 45th Gaseous Electronics Conf. (Boston, MA, 27–30 October 1992)*

[30] Gorbatkin M, Berry L A and Roberto J B 1990 Behavior of Ar plasmas formed in a mirror field electron cyclotron resonance microwave ion source *J. Vac. Sci. Technol.* **A8** 2893

[31] Rossnagel S M, Whitehair S J, Guarnieri C R and Cuomo J J 1990 Plasma induced gas heating in electron cyclotron resonance sources *J. Vac. Sci. Technol.* **A8** 3113

[32] Nakano T, Sadeghi N and Gottscho R A 1991 Ion and neutral temperatures in electron cyclotron resonance plasma reactors *Appl. Phys. Lett.* **58** 458

[33] Hartig M J and Kushner M J 1993 Monte Carlo hydrodynamic simulation of neutral radical transport in low pressure remote plasma activated chemical vapor deposition *Appl. Phys. Lett.* **62** 1594

[34] Kilgore M D, Wu H M and Graves D B 1994 Neutral transport in high plasma density reactors *J. Vac. Sci. Technol.* B **12** 494

[35] Hebner G A 1996 Spatially resolved, excited state densities and neutral and ion temperatures in inductively coupled argon plasma *J. Appl. Phys.* **80** 2624

[36] Hori T, Bowden M D, Uchino K, Muraoka K and Maeda M 1996 Measurements of electron temperature, electron density and neutral density in a radiofrequency inductively coupled plasma *J. Vac. Sci. Technol.* A **14** 144

[37] Lee P W and Chang H Y 1996 Interpretation of neutral distribution through spatial profile of plasma emission *Phys. Lett.* A **213** 186

[38] Sudit I D and Chen F F 1996 Discharge equilibrium of a helicon plasma *Plasma Sources Sci. Technol.* **5** 43

[39] Chen F F, Sudit I D and Light M 1996 Downstream physics of the helicon discharge *Plasma Sources Sci. Technol.* **5** 173

[40] Gilland J J, Breun R and Hershkowitz N 1998 Neutral pumping in a helicon discharge *Plasma Sources Sci. Technol.* **7** 416

[41] Miljak D G and Chen F F 1998 Density limit in helicon discharges *Plasma Sources Sci. Technol.* **7** 537

[42] Degeling A W, Sheridan T E and Boswell R W 1999 Model for relaxation oscillations in a helicon discharge *Phys. Plasmas* **6** 1641

[43] Degeling A W, Sheridan T E and Boswell R W 1999 Intense on-axis plasma production and associated relaxation oscillations in a large volume helicon source *Phys. Plasmas* **6** 3664

[44] Booth J-P, Cunge G, Chabert P and Sadeghi N 1999 CF_x radical production and loss in a CF_4 reactive ion etching plasma: fluorine rich conditions *J. Appl. Phys.* **85** 3097

[45] Fiala A, Kiehlbauch M, Mahnovski S and Graves D B 1999 Model of point-of-use plasma abatement of perfluorinated compounds with an inductively coupled plasma *J. Appl. Phys.* **86** 152

[46] Tynan G R 1999 Neutral depletion and transport mechanism in large-area high density plasma sources *J. Appl. Phys.* **86** 5356

[47] Cho S 1999 A self-consistent global model of neutral gas depletion in pulsed helicon plasmas *Phys. Plasmas* **6** 359

[48] Yun S, Taylor K and Tynan G R 2000 Measurement of radial neutral pressure and plasma density profiles in various plasma conditions in large-area high-density plasma sources *Phys. Plasmas* **7** 3448

[49] Donnelly V M and Malyshev M V 2000 Diagnostics of inductively coupled chlorine plasmas: Measurements of the neutral gas temperature *Appl. Phys. Lett.* **77** 2467

[50] Hebner G A 2001 CF, CF_2 and SiF densities in inductively driven discharges containing C_2F_6, C_4F_8 and CHF_3 *J. Appl. Phys.* **89** 900

[51] Singh H, Coburn J W and Graves D B 2001 Measurements of neutral and ion composition, neutral temperature and electron energy distribution function in a CF_4 inductively coupled plasma *J. Vac. Sci. Technol.* **A19** 718

[52] Kiehlbauch M W and Graves D B 2001 Temperature resolved modeling of plasma abatement of perfluorinated compounds *J. Appl. Phys.* **89** 2047

[53] Bellini M, Corsi C and Gambino M C 2001 Neutral depletion and beam defocusing in harmonic generation from strongly ionized media *Phys. Rev.* A **64** 023411

[54] Tonnis E J and Graves D B 2002 Neutral gas temperatures measured within a high-density, inductively coupled plasma abatement device *J. Vac. Sci. Technol.* A **20** 1787

[55] Abada H, Chabert P, Booth J P, Robiche J and Gartry G 2002 Gas temperature gradients in a CF_4 inductive discharge *J. Appl. Phys.* **92** 4223

[56] Liu M, Hu X, Yu G, Wu Q and Pan Y 2002 Two-dimensional simulation of an electron cyclotron resonance plasma source with power deposition and neutral gas depletion *Plasma Sources Sci. Technol.* **11** 260

[57] Gans T, Schulz-von der Gathen V, Czarnetzki U and Dobele H F 2002 Observation of fast hydrogen atoms formed by ion bombarding of surfaces *Contrib. Plasma Phys.* **42** 596

[58] Okamoto A, Hara K, Nagaoka K, Yoshimura S, Vranjes J, Kono M and Tanaka M Y 2003 Experimental observation of a tripolar vortex in a plasma *Phys. Plasmas* **10** 2211

[59] Clarenbach B, Lorenz B, Kramer M and Sadeghi N 2003 Time-dependent gas density and temperature measurements in pulsed helicon discharges in argon *Plasma Sources Sci. Technol.* **12** 345

[60] Watts C and Hanna J 2004 Alfvèn wave propagation in a partially ionized plasma *Phys. Plasmas* **11** 1358

[61] Shimada M, Cattolica R and Tynan G R 2004 Electron beam fluorescence temperature measurements of N_2 in a semiconductor plasma reactor *J. Vac. Sci. Technol.* **A 22** 371

[62] Fruchtman A, Makrinich G, Chabert P and Rax J M 2005 Enhanced plasma transport due to neutral depletion *Phys. Rev. Lett.* **95** 115002

[63] Kushner M J 2005 Modelling of microdischarge devices: plasma and gas dynamics *J. Phys. D: Appl. Phys.* **38** 1633

[64] Abdel-Rahman M, Gans T, Schulz-von der Gathen V and Dobele H F 2005 Space and time resolved rotational state populations and gas temperatures in an inductively coupled hydrogen RF discharge *Plasma Sources Sci. Technol.* **14** 51

[65] Dunaevsky A, Raitses Y and Fisch N J 2006 Plasma acceleration from radio-frequency discharge in dielectric capillary *Appl. Phys. Lett.* **88** 251502

[66] Makrinich G and Fruchtman A 2006 Heat flux measurements and plasma composition *J. Appl. Phys.* **100** 093302

[67] Shimada M, Tynan G R and Cattolica R 2006 Rotational and translational temperature equilibrium in an inductively coupled plasma *J. Vac. Sci. Technol.* A **24** 1878

[68] Keesee A M and Scime E E 2006 Neutral argon density profile determination by comparison of spectroscopic measurements and a collisional-radiative model *Rev. Sci. Instrum.* **77** 10F304

[69] O'Connell D, Gans T, Crintea D, Czarnetzki U and Sadeghi N 2006 *Proc. of the 59th Annual Gaseous Electronics Conf. (10–13 October 2006) p* 002

[70] Keesee A M and Scime E E 2007 Neutral density profiles in argon helicon plasmas *Plasma Sources Sci. Technol.* **16** 742

[71] Clarenbach B, Kramer M and Lorenz B 2007 Spectroscopic investigations of electron heating in a high-density helicon discharge *J. Phys. D: Appl. Phys.* **40** 5117

[72] Raimbault J-L, Liard L, Rax J-M, Chabert P, Fruchtman A and Makrinich G 2007 Steady-state isothermal bounded plasma with neutral dynamics *Phys. Plasmas* **14** 013503

[73] Maggs J E, Carter T A and Taylor R J 2007 Transition from Bohm to classical diffusion due to edge rotation of a cylindrical plasma *Phys. Plasmas* **14** 052507

[74] Liard L, Raimbault J-L, Rax J-M and Chabert P 2007 Plasma transport under neutral gas depletion conditions *J. Phys. D: Appl. Phys.* **40** 5192

[75] Aanesland A, Liard L, Leray G, Jolly J and Chabert P 2007 Direct measurements of neutral density depletion by two-photon absorption laser-induced fluorescence spectroscopy *Appl. Phys. Lett.* **91** 121502

[76] Shimada M, Tynan G R and Cattolica R 2007 Neutral gas density depletion due to neutral gas heating and pressure balance in an inductively coupled plasma *Plasma Sources Sci. Technol.* **16** 193

[77] Fruchtman A 2008 Neutral depletion in a collisionless plasma *IEEE Trans. Plasma Science* **36** 403

[78] Fruchtman A 2008 Energizing and depletion of neutrals by a collisional plasma *Plasma Sources Sci. Technol.* **17** 024016

[79] Fruchtman A, Makrinich G, Raimbault J-L, Liard L, Rax J-M and Chabert P 2008 Neutral depletion versus repletion due to ionization *Phys. Plasmas* **15** 057102

[80] Shimada M, Tynan G R and Cattolica R 2008 Neutral depletion in inductively coupled plasmas using hybrid-type direct simulation method *J. Appl. Phys.* **103** 033304

[81] O'Connell D, Gans T, Crintea D L, Czarnetzki U and Sadeghi N 2008 Neutral gas depletion mechanisms in dense low-temperature argon plasmas *J. Phys. D: Appl. Phys.* **41** 035208

[82] O'Connell D, Gans T, Crintea D L, Czarnetzki U and Sadeghi N 2008 Plasma dynamics in an inductively coupled magnetic neutral loop discharge *Plasma Sources Sci. Technol.* **17** 024022

[83] Denning C M, Wiebold M and Scharer J E 2008 Observations of neutral depletion and plasma acceleration in a flowing high-power argon helicon plasma *Phys. Plasmas* **15** 072115

[84] Taccogna F, Schneider R, Matyash K, Longo S, Capitelli M and Tshakaya D 2008 Plasma-neutral interaction in kinetic models for the divertor region *Contrib. Plasma Phys.* **48** 147

[85] Fruchtman A 2009 Ambipolar and nonambipolar cross-field diffusions *Plasma Sources Sci. Technol.* **18** 025033

[86] Liard L, Raimbault J-L and Chabert P 2009 Competitive effects of an axial magnetic field and of neutral gas depletion in a positive column *Phys. Plasmas* **16** 053507

[87] Crintea D L, Czarnetzki U, Iordanova S, Koleva I and Luggenholscher D 2009 Plasma diagnostics by optical emission spectroscopy on argon and comparison with Thomson scattering *J. Phys. D: Appl. Phys.* **42** 045208

[88] Fruchtman A 2010 Nonmonotonic plasma density profile due to neutral-gas depletion *Phys. Plasmas* **17** 023502

[89] Fruchtman A and Rax J-M 2010 Neutral-gas depletion and repletion in plasmas *Phys. Plasmas* **17** 043502

[90] Fruchtman A 2011 The thrust of a collisional plasma source *IEEE Trans. Plasma Sci.* **39** 530

[91] Hagelaar G J M, Fubiani G and Boeuf J P 2011 Model of an inductively coupled negative ion source: I. General model description *Plasma Sources Sci. Technol.* **20** 015001

[92] Boeuf J P, Hagelaar G J M, Sarrailh P, Fubiani G and Kohen N 2011 Model of an inductively coupled negative ion source: II. Application to an ITER type source *Plasma Sources Sci. Technol.* **20** 015002

[93] McNeely P, Wunderlich D and The NNBI Team 2011 Neutral depletion in an H^- source operated at high RF power and low input gas flow *Plasma Sources Sci. Technol.* **20** 045005

[94] Curreli D and Chen F F 2011 Equilibrium theory of cylindrical discharges with special application to helicons *Phys. Plasmas* **18** 113501

[95] Houshmandyar S and Scime E E 2012 Enhanced neutral depletion in a static helium helicon discharge *Plasma Sources Sci. Technol.* **21** 035008

[96] Magee R M, Galante M E, Gulbrandsen N, McCarren D W and Scime E E 2012 Direct measurements of the ionization profile in krypton helicon plasmas *Phys. Plasmas* **19** 123506

[97] Liard L, Aanesland A and Chabert P 2012 Dynamics of neutral gas depletion investigated by time- and space-resolved measurements of xenon atom ground state density *J. Phys. D: Appl. Phys.* **45** 235201

[98] Magee R M, Galante M E, Carr J Jr, Lusk G, McCarren D W and Scime E E 2013 Neutral depletion and the helicon density limit *Phys. Plasmas* **20** 123511

[99] Cooper C M and Gekelman W 2013 Termination of a magnetized plasma on a neutral gas: the end of the plasma *Phys. Rev. Lett.* **110** 265001

[100] Charles C, Dedrick J, Boswell R W, O'Connell D and Gans T 2013 Nanosecond optical imaging spectroscopy of an electrothermal radiofrequency plasma thruster plume *Appl. Phys. Lett.* **103** 124103

[101] Giannelli S, Kieckhafer A and Walker M L R 2013 Neutral gas expansion in a cylindrical helicon discharge chamber *J. Propulsion Power* **29** 540

[102] Greig A, Charles C, Paulin N and Boswell R W 2014 Volume and surface propellant heating in an electrothermal radio-frequency plasma micro-thruster *Appl. Phys. Lett.* **105** 054102

[103] Wunderlich D, Mochalskyy S, Fantz U, Franzen P and The NNBI-Team 2014 Modelling the ion source for ITER NBI: from the generation of negative hydrogen ions to their extraction *Plasma Sources Sci. Technol.* **23** 015008

[104] Gaboriau F and Boeuf J P 2014 Chemical kinetics of low pressure high density hydrogen plasmas: application to negative ion sources for ITER *Plasma Sources Sci. Technol.* **23** 065032

[105] Yamamoto T, Shibata T, Ohta M, Yasumoto M, Nishida K, Hatayama A, Mattei S, Lettry J, Sawada K and Fantz U 2014 Modeling of neutrals in the Linac4 H^- ion source plasma: hydrogen atom production density profile and H_α intensity by collisional radiative model *Rev. Sci. Instrum.* **85** 02B118

[106] Galante M E, Magee R M and Scime E E 2014 Two photon absorption laser induced fluorescence measurements of neutral density in a helicon plasma *Phys. Plasmas* **21** 055704

[107] Curreli D and Chen F F 2014 Cross-field diffusion in low-temperature plasma discharges of finite length *Plasma Sources Sci. Technol.* **23** 064001

[108] Ding Ke, Lieberman M A and Lichtenberg A J 2014 Hybrid model of neutral diffusion, sheaths and the α to γ transition in an atmospheric pressure He/H_2O bounded rf discharge *J. Phys. D: Appl. Phys.* **47** 305203

[109] Takahashi K, Chiba A, Komuro A and Ando A 2015 Axial momentum lost to a lateral wall of a helicon plasma source *Phys. Rev. Lett.* **114** 195001

[110] Valentini H-B and Kaiser D 2015 The limits of the Bohm criterion in collisional plasmas *Phys. Plasmas* **22** 053512

[111] Takahashi K, Takao Y and Ando A 2016 Neutral-depletion-induced axially asymmetric density in a helicon source and imparted thrust *Appl. Phys. Lett.* **108** 074103

[112] Simon A 1955 *Phys. Rev.* **98** 317
Simon A 1958 *Int. Conf. on the Peaceful Uses of Atomic Energy* vol 33, 2nd edn (Geneva: United Nations) p 343

[113] Baalrud S D, Hershkowitz N and Longmier B 2007 *Phys. Plasmas* **14** 042109

[114] Shinohara S, Kuwahara D, Yano K and Fruchtman A 2016 *Phys. Plasma* **23** 122108

[115] Charles C 2009 Plasmas for spacecraft propulsion *J. Phys. D: Appl. Phys.* **42** 163001.

[116] Makrinich G and Fruchtman A 2009 Enhancement of electric force by ion–neutral collisions *Appl. Phys. Lett.* **95** 181504

[117] Huang W S, Gallimore A D and Hofer R R 2011 Neutral flow evolution in a six-kilowatt Hall thruster *J. Propulsion Power* **27** 553

[118] Charles C, Boswell R and Takahashi K 2012 Investigation of radiofrequency plasma sources for space travel *Plasma Phys. Control. Fusion* **54** 1

[119] Greig A, Charles C, Hawkins R and Boswell R 2013 Direct measurement of neutral gas heating in a radio-frequency electrothermal plasma micro-thruster *Appl. Phys. Lett.* **103** 074101

[120] Makrinich G and Fruchtman A 2013 Enhanced momentum delivery by electric force to ions due to collisions of ions with neutrals *Phys. Plasmas* **20** 043509

[121] Ahedo E and Navarro-Cavalle J 2013 Helicon thruster plasma modeling: two-dimensional fluid-dynamics and propulsive performances *Phys. Plasmas* **20** 043512

[122] Little J M and Choueiri E Y 2013 Thrust and efficiency model for electron-driven magnetic nozzles *Phys. Plasmas* **20** 103501

[123] Lafleur T 2014 Helicon plasma thruster discharge model *Phys. Plasmas* **21** 043507

[124] Shinohara S, Nishida H, Tanikawa T, Hada T, Funaki I and Shamrai K P 2014 Development of electrodeless plasma thrusters with high density helicon plasma sources *IEEE Trans. Plasma Sci.* **42** 1245

[125] Sheehan J P *et al* 2014 Temperature gradients due to adiabatic plasma expansion in a magnetic nozzle *Plasma Sources Sci. Technol.* **23** 045014

[126] Fruchtman A 2015 Enhanced thrust due to ion–neutral collisions for electric propulsion *Plasma Chem. Plasma Process.* **34** 647

[127] Merino M and Ahedo E 2015 Influence of electron and ion thermodynamics on the magnetic nozzle plasma expansion *IEEE Trans. Plasma Sci.* **43** 244

[128] Williams L T and Walker M L R 2015 Plume structure and ion acceleration of a helicon plasma source *IEEE Trans. Plasma Sci.* **43** 1694

[129] Otsuka S, Takizawa K, Tanida Y, Kuwahara D and Shinohara S 2015 Study on plasma acceleration in completely electrodeless electric propulsion system *Plasma Fusion Res.* **10** 3401026

[130] Charles C, Bish A, Boswell R W, Dedrick J, Greig A, Hawkins R and Ho T S 2016 A short review of experimental and computational diagnostics for radiofrequency plasma micro-thrusters *Plasma Chem. Plasma Process.* **36** 29

[131] Lukas J, Teel G, Kolbeck J and Keidar M 2016 High thrust-to-power ratio micro-cathode arc thruster *AIP Adv.* **6** 025311

[132] Mazouffre S 2016 Electric propulsion for satellites and spacecraft: established technologies and novel approaches *Plasma Sources Sci. Technol.* **25** 033002

[133] Rafalskyi D and Aanesland A 2016 Brief review on plasma propulsion with neutralizer-free systems *Plasma Sources Sci. Technol.* **25** 043001

[134] Vlcek J 1989 A collisional-radiative model applicable to argon discharges over a wide range of conditions. I. Formulation and basic data *J. Phys. D: Appl. Phys.* **22** 623

[135] Bogaerts A, Gijbels R and Vlcek J 1998 Collisional-radiative model for an argon glow discharge *J. Appl. Phys.* **84** 121

[136] Gudmundsson J T 2002 *Technical Report* RH-21-2002, Science Institute, University of Iceland, Reykjavik, Iceland
Hjartarson A T, Thorsteinsson E G and Gudmundsson J T 2010 Low pressure hydrogen discharges diluted with argon explored using a global model *Plasma Sources Sci. Technol.* **19** 065008

[137] Finlay-Freundlich E 1958 *Celestial Mechanics* (New York: Pergamon) p 72

[138] Averbukh I Sh and Arvieu R 2001 *Phys. Rev. Lett.* **87** 163601

[139] Golant V, Zhilinsky A P, Sakharov I E and Brown S C 1980 *Fundamentals of Plasma Physics* (New York: Wiley)

[140] Murray J D 1984 *Asymptotic Analysis* (New York: Springer) ch 2

[141] Phelps A V 1991 Cross sections and swarm coefficients for nitrogen ions and neutrals in N_2 and argon ions and neutrals in Ar for energies from 0.1 eV to 10 keV *J. Phys. Chem. Ref. Data* **20** 557

[142] Fruchtman A and Shinohara S 2017 *Phys. Plasmas* **24** 103523